



OPEN

Synthesis, spectroscopic, DFT calculations, biological activity, SAR, and molecular docking studies of novel bioactive pyridine derivatives

Kurls E. Anwer¹, Zeinab K. Hamza² & Ramadan M. Ramadan¹✉

Enaminonitrile pyridine derivative was used as a precursor for preparation of fourteen heterocyclic compounds using both conventional thermal and microwave techniques. Diverse organic reagents, such as chloroacetyl chloride, acetic anhydride, chloroacetic acid, carbon disulfide, *p*-toluene sulfonyl chloride, maleic anhydride, phthalic anhydride, were used. The chemical formulae and structures of isolated derivatives were obtained using different analytical and spectroscopic techniques such as IR, ¹H-, ¹³C-NMR as well as mass spectrometry. The spectroscopic analyses revealed diverse structure arrangements for the products. Molecular structure optimization of certain compounds were performed by the density functional theory (DFT/B3LYP) method and the basis set 6–31 G with double zeta plus polarization (d,p). The antimicrobial inhibition and the antioxidant activity of the reported compounds were screened. Compounds 5, 6, 11 and 13 exhibited the highest antibacterial inhibition, while compound 8 gave the highest scavenging activity (IC₅₀ 43.39 µg/ml) against the DPPH radical. Structure–activity relationship of the reported compounds were correlated with the data of antibacterial and the antioxidant activity. The global reactivity descriptors were also correlated with the biological properties of compounds. The molecular docking studies of reported compounds were investigated, and the analysis showed that the docked compounds have highly negative values for the functional binding scores. The binding interaction was found to be correlated with the substituent fragments of the compounds.

Heterocyclic derivatives containing nitrogen such as azines and pyridine frameworks are important derivatives in both chemistry and biology, and they are commonly used in pharmaceuticals, vitamins, natural products and functional reagents syntheses^{1–5}. It is known that pyridine derivatives have improved therapeutic properties. These particular properties have grafted the organic researchers to pay more attention on the key molecule with different geometries, which determine possible interactions with a specific protein or DNA, and define the biological selectivity for the target molecule⁶. Pyridine derivatives are widely reported as potential anticancer⁷, antibacterial⁸, anti-fibrotic agents⁹, anti-inflammatory¹⁰, cardiotonic¹¹, IKK-β inhibitors¹² and HIV-1 inhibitor¹³. From these derivatives, 2-amino-3-cyanopyridine is considered a bioactive essential supporting material to design layout structures for promising new drugs. The high reactivity of the 2-amino-3-cyanopyridine scaffold illustrated that it can be used to prepare many reactive organic intermediates used to produce nicotinamides and many pharmaceutical drugs like Ridogrel and Pirenzepine^{14,15}. Furthermore, substitution of phenyl or aryl moieties in the fourth and sixth position of 2-amino-3-cyanopyridine, was found to enhance the biological activities of these products. For example, derivatives of 2-amino-3-cyano-6-(1H-indol-3-yl)-4-phenylpyridine were found to be cytotoxic against different human tumors cell. The pharmacological investigations proved that introduction indole core improved the antitumor activities of 4,6-diaryl-2-amino-3-cyanopyridines¹⁶. Moreover, derivatives of pyrimidine and pyridine such as substituted 2,6-diaryl- and 3,4-dihydropyrimidinone exhibited appropriate cytotoxic effects against several cancer cell lines, which reflected the potential application of these compounds to modify and develop more selective anticancer agents¹⁷. On the other hand, these derivatives

¹Department of Chemistry, Faculty of Science, Ain Shams University, Cairo, Egypt. ²Food Toxicology and Contaminants Department, National Research Centre, Giza, Egypt. ✉email: r_m_ramadan@yahoo.com

and related ones showed very interesting spectroscopic properties and fluorescent effects, which have many important applications^{18,19}.

Because of the sound biological activities of this category of derivatives, many reports appeared to develop the synthesis of novel pyridine derivatives using either conventional or microwave irradiation methods. Notably, the microwave irradiation recently gained much attention and considered as one of the preferred green chemistry tools because of its capability in improving the obtained yield and reducing the reaction times as well as it is environmentally safe^{20,21}.

Our interest in synthesis of nitrogen-based heterocyclic derivatives that have prominent biological activity^{20,22–24} encouraged us to synthesize a series of pyridine derivative that could have potential bioactivity. Here, we report the synthesis of an enamionitrile pyridine, 2-amino-6-(2,4-dimethoxyphenyl)-4-phenylnicotinonitrile, along with its reactions with some selected reagents. Different structure arrangements were concluded from the analytical and spectroscopic studies. The reported derivatives were identified by using different spectroscopic and analytical techniques along with theoretical DFT calculations and molecular docking analysis. The antimicrobial and antioxidant activities of the reported derivatives also showed that some derivatives have potent inhibition towards the screened microorganisms. Structure–activity relationships (SAR) of the different products are correlated with the biological studies and the theoretical findings.

Experimental

Reagents and instruments. The chemicals and reagents for this study were of analytical reagents and supplied by Sigma Aldrich. Solvents used were purified by the known standard methods. Thin layer chromatography (TLC) experiments were carried out on precoated silica gel plates purchased from Merck Kiesel gel 60F 254, BDH. Digital Stuart SMP3 electric melting point equipment was used to measure the melting points of the compounds. The microwave irradiation reactions (10 mL borosilicate glass vials) were performed using Anton Paar (monowave 300) microwave reactor. Mass spectrometry (EI, 70 eV) measurements were performed on a GC-2010 Shimadzu GCM spectrometer. Perkin-Elmer 293 spectrophotometer instrument was used for the IR measurements (KBr pellets, cm⁻¹). ¹H- and ¹³C-NMR measurements had been performed on a Varian Mercury 300 MHz spectrometer. Deuterated DMSO solutions of the samples with TMS as internal standard were used for the analysis. The microanalytical (CHN) analyses were carried out using a Perkin-Elmer analyzer (CHN-2400). Accuracy of the data were within ± 0.3% of calculated values.

Syntheses procedures of the compounds. *2-Amino-6-(2,4-dimethoxyphenyl)-4-phenylnicotinonitrile (1)*. Equimolar mixture of benzaldehyde (0.01 mol, 1.09 mL), malononitrile (0.01 mol, 0.66 g), 2,4-dimethoxyacetophenone (0.01 mol, 1.8 g) with CH₃COONH₄ (0.015 mol, 1.16 g) was fused at 100 °C for a time period of 5h. Reaction mixture was cooled, and the obtained residue was washed with water several times and then recrystallized using hot alcohol. Yield: Conventional heating, 70%; Microwave radiation, 93%.

General procedure for the synthesis of the compounds 2–15. A solution of a mixture of compound **1** (0.01 mol, 3.31 g) and the relevant reagent in the selected solvent was heated to reflux. Reaction mixture was cooled and decanted in crushed ice (~ 100 g). The precipitated residue was collected and then recrystallized from hot methanol.

** Reagents for the synthesis of compounds 2–15.

(2) 2-chloro-N-(3-cyano-6-(2,4-dimethoxyphenyl)-4-phenylpyridin-2-yl)acetamide: Chloroacetyl chloride (1.12 mL)/DMF (30 mL)/18h. Yield: Conventional heating, 72%; Microwave radiation, 90%.

(3) 2-Cyano-N-(3-cyano-6-(2,4-dimethoxyphenyl)-4-phenylpyridin-2-yl)acetamide: Cyano acetic acid (0.85 g)/acetic anhydride (30 mL)/12h. Yield: Conventional heating, 77%; Microwave radiation, 91%.

(4) N-acetyl-N-(3-cyano-6-(2,4-dimethoxyphenyl)-4-phenylpyridin-2-yl)acetamide: Acetic anhydride (30 mL)/24h. Yield: Conventional heating, 71%; Microwave radiation, 93%.

(5) Ethyl-N-(3-cyano-6-(2,4-dimethoxyphenyl)-4-phenylpyridin-2-yl)formimidate: Triethyl orthoformate (10 mL)/20h. Yield: Conventional heating, 74%; Microwave radiation, 90%.

(6) 6-(2,4-Dimethoxyphenyl)-2-(methylamino)-4-phenylnicotinonitrile: Chloroacetic acid (0.94 g)/pyridine (20 mL)/19h. Yield: Conventional heating, 76%; Microwave radiation, 94%.

(7) 6-(2,4-Dimethoxyphenyl)-2-isothiocyanato-4-phenylnicotinonitrile: Carbon disulphide (30 mL)/28h. Yield: Conventional heating, 77%.

(8) N-(3-Cyano-6-(2,4-dimethoxyphenyl)-4-phenylpyridin-2-yl)-4-methylbenzenesulfonamide: *p*-Toluene sulfonyl chloride (1.9 g)/butanol (30 mL)/10h/recrystallized from hot benzene. Yield: Conventional heating, 70%; Microwave radiation, 90%.

(9) 6-(2,4-Dimethoxyphenyl)-2-(2,5-dioxo-2,5-dihydro-1H-pyrrol-1-yl)-4-phenylnicotinonitrile: Maleic anhydride (0.98 g)/acetic acid (30 mL)/16h. Yield: Conventional heating, 74%; Microwave radiation, 88%.

(10) 6-(2,4-Dimethoxyphenyl)-2-(1,3-dioxoisindolin-2-yl)-4-phenylnicotinonitrile: Phthalic anhydride (1.48 g)/acetic acid (30 mL)/17h. Yield: Conventional heating, 72%; Microwave radiation, 92%.

(11) 7-(2,4-Dimethoxyphenyl)-5-phenylpyrido[2,3-d]pyrimidin-4-amine: Formamide (30 mL)/20h. Yield: Conventional heating, 73%; Microwave radiation, 87%.

(12) 4-amino-7-(2,4-dimethoxyphenyl)-2,5-diphenyl-1,8-naphthyridine-3-carbonitrile: Benzylidene malononitrile (1.54 g)/butanol (30 mL)/24h/recrystallized from hot dioxane. Yield: Conventional heating, 77%; Microwave radiation, 89%.

(13) 4-Amino-7-(2,4-dimethoxyphenyl)-2-hydroxy-5-phenyl-1,8-naphthyridine-3-carbonitrile: Ethyl cyanoacetate (1.13 mL)/drops of piperidine/DMF (30 mL)/17h. Yield: Conventional heating, 73%; Microwave radiation, 87%.

(14) 2,4-Diamino-7-(2,4-dimethoxyphenyl)-5-phenyl-1,8-naphthyridine-3-carbonitrile: Malononitrile (0.66 g)/drops of piperidine/butanol (30 mL)/10h. Yield: Conventional heating, 71%; Microwave radiation, 90%.

(15) 7-(2,4-Dimethoxyphenyl)-2-methyl-5-phenylpyrido[2,3-d]pyrimidin-4(3H)-one: Few drops of conc. sulphuric acid/acetic anhydride (30 mL)/15h/recrystallized from hot acetone. Yield: Conventional heating, 72%; Microwave radiation, 90%.

Table 1 gives the melting points, elemental analyses and mass spectral data for all derivatives.

Molecular orbital calculations. Molecular orbital computation was performed using the software package of Gaussian 09W²⁵. DFT (B3LYP) method and the basis set 6-31G (d,p) with double zeta plus polarization for carbon, hydrogen, nitrogen, oxygen, sulfur and chloride was applied.

Biological activity studies. *Antimicrobial activity.* In vitro evaluation of the reported compounds for their antimicrobial activities (agar well diffusion method) was performed. The experimental procedures of the studies were as described in previous report²⁶. The antibacterial screening of the compounds was against three gram-negative bacteria (*Escherichia coli*, *Salmonella typhimurium* and *Yersinia enterocolitica*) and two gram-positive bacteria (*Staphylococcus aureus* and *Bacillus cereus*). For the antibacterial activity, Cefoperazone was served as a standard. The antifungal activities were checked on three fungi (*Aspergillus flavus*, *Aspergillus niger* and *Fusarium oxysporum*). Analyses for every compound were performed in triplicate measurements and the average values are reported.

Antioxidant study. Scavenging modeling of the stable radical 2,2-diphenyl-1-picrylhydrazyl (DPPH) is employed to determine antioxidant activity of tested derivatives²⁶. 1.0 mM stock solution of DPPH was prepared in methanol. Solutions of different concentrations (25–200 $\mu\text{g mL}^{-1}$) from ascorbic acid and the tested compounds were prepared using DMSO. 1.0 mL of the sample solution was mixed with 3.0 mL (0.1 mM) of DPPH. Incubation of the samples at room temperature for 30 min. Control experiment was performed without the tested samples. Measurements of the absorbance at 517 nm of the tested solutions were performed. As the concentration of the tested compounds increased, a marked decrease in the absorption was observed. This remarkable decrease indicated strong antioxidant activity of the compounds. The DPPH was a positive control, DMSO was a negative control and ascorbic acid was a standard. Reduction of DPPH was estimated relative to measured absorbance of the control. The measurements were carried out in triplicates. Percentage of the radical scavenging was computed using the relation:

$$\% \text{Radical scavenging activity} = \frac{A_c - A_s}{A_s}$$

Absorbance of control reaction having all reagents excepting the tested compounds is given A_c . Absorbance of sample at any concentration C is denoted A_s . Effective concentrations of the sample desired for scavenging 50% (IC_{50} value) of DPPH radical was obtained by plotting the percentage of inhibition versus concentrations with the use of linear regression analysis.

Compound	m.p., °C	Elemental analysis, Found (Calcd.)			Mass spectrometry	
		% C	% H	% N	M.M	m/z
C ₂₀ H ₁₇ N ₅ O ₂ (1)	230–232	72.27 (72.49)	5.06 (5.17)	12.72 (12.68)	331.38	331 [P ⁺] (24.92%)
C ₂₂ H ₁₈ ClN ₅ O ₃ (2)*	150–152	64.83 (64.79)	4.38 (4.45)	10.41 (10.30)	407.85	407 [P ⁺] (13.05%)
C ₂₃ H ₁₈ N ₄ O ₃ (3)	188–190	69.25 (69.34)	4.61 (4.55)	14.23 (14.06)	398.42	398 [P ⁺] (20.26%)
C ₂₄ H ₂₁ N ₅ O ₄ (4)	146–148	69.21 (69.39)	5.47 (5.10)	10.16 (10.11)	415.45	415 [P ⁺] (20%)
C ₂₃ H ₂₁ N ₅ O ₃ (5)	> 300	71.15 (71.30)	5.29 (5.46)	10.92 (10.85)	387.44	387 [P ⁺] (24%)
C ₂₁ H ₁₉ N ₅ O ₂ (6)	250–252	73.12 (73.03)	5.41 (5.54)	12.02 (12.17)	345.40	345 [P ⁺] (18.05%)
C ₂₁ H ₁₅ N ₅ O ₂ S (7)**	> 300	67.35 (67.54)	4.14 (4.05)	11.07 (11.25)	373.43	373 [P ⁺] (55.07%)
C ₂₇ H ₂₃ N ₅ O ₄ S (8)***	> 300	66.68 (66.79)	4.82 (4.77)	8.77 (8.65)	485.56	485 [P ⁺] (18.0%)
C ₂₄ H ₁₇ N ₅ O ₄ (9)	168–170	70.16 (70.07)	4.28 (4.17)	10.39 (10.21)	411.42	411 [P ⁺] (46.77%)
C ₂₈ H ₁₉ N ₅ O ₄ (10)	280–282	72.98 (72.88)	4.03 (4.15)	9.07 (9.11)	461.48	461 [P ⁺] (9.29%)
C ₂₁ H ₁₈ N ₄ O ₂ (11)	> 300	70.42 (70.38)	5.14 (5.06)	15.42 (15.63)	358.40	358 [P ⁺] (23.33%)
C ₂₉ H ₂₂ N ₄ O ₂ (12)	> 300	75.88 (75.97)	4.58 (4.84)	12.31 (12.22)	458.52	458 [P ⁺] (15.8%)
C ₂₃ H ₁₈ N ₄ O ₃ (13)	> 300	69.42 (69.34)	4.46 (4.55)	14.12 (14.06)	398.42	398 [P ⁺] (12.43%)
C ₂₃ H ₁₉ N ₅ O ₂ (14)	192–194	69.59 (69.51)	4.75 (4.82)	17.66 (17.62)	397.44	397 [P ⁺] (16.25%)
C ₂₂ H ₁₉ N ₅ O ₃ (15)	262–264	70.68 (70.76)	5.02 (5.13)	11.44 (11.25)	373.41	373 [P ⁺] (14.47%)

Table 1. Elemental analyses and mass spectrometry data for the reported compounds. *% Cl, 8.51 (8.69); **% S, 8.64 (8.59); ***% S, 6.59 (6.60).

Molecular docking studies. Docking studies were carried out using Molecular Operating Environment (MOE) package version 2014.0901. Structure of a B-DNA (X-ray crystal structure) with the code PDB ID: 1BNA was downloaded from Research Collaboratory for Structural Bioinformatics (RCSB) database.

Results and discussion

The synthesis of compounds and spectroscopic studies. The enamionitrile pyridine derivative, 2-amino-6-(2,4-dimethoxyphenyl)-4-phenylnicotinonitrile (**1**), was prepared using either thermal or microwave irradiation techniques. It was proceeded via a four-component one-pot reaction including benzaldehyde, 2,4-dimethoxy acetophenone, malononitrile, and ammonium acetate (Fig. 1). Structure of **1** was elucidated by elemental analyses and mass spectrometry (Table 1) and the IR, ^1H - and ^{13}C -NMR spectroscopic tools (Table 2). Compound **1** displayed a signal at m/z 331 in its mass spectrum due to the molecular peak. Infrared spectrum of **1** displayed the different functional groups in their expected positions. It exhibited two asymmetric and symmetric stretching frequencies for NH_2 group at 3460 and 3369 cm^{-1} . In addition, a strong vibrational stretching frequency at 2207 cm^{-1} was assigned for the $\text{C}\equiv\text{N}$ moiety²⁷. In the ^1H -NMR spectrum of **1**, the NH_2 protons exhibited a broad signal at 7.26 ppm, Fig. 1S (A). This signal disappeared on addition of D_2O to the solution and indicated that the protons of NH_2 are exchangeable with the deuterium of D_2O , Fig. 1S (B). Furthermore, the ^1H -NMR spectrum of **1** showed signals due to the OCH_3 and aromatic protons. The ^{13}C -NMR spectrum of **1**, on the other hand, showed a set of signals due to carbon atoms in their appropriate positions (Fig. 2S and Table 2). As expected, the signals of the two OCH_3 carbon atoms appeared at higher field (56.4 and 58.6 ppm). In addition, the signals of the pyridine carbon attached to the $\text{C}\equiv\text{N}$ group and the signal of the cyano carbon itself also occurred at their anticipated positions (109.8 and 112.4 ppm). Figure 2 displayed a speculated mechanism for formation of the precursor **1**.

It was found that compound **1** is a reactive derivative and can react with a diverse number of reagents. It reacted with either chloroacetyl chloride, cyanoacetic acid or acetic anhydride to give 2-chloro-acetamide, 2-cyano-acetamide, and N-acetyl-acetamide pyridine derivatives (**2–4**), respectively (Fig. 3). Interestingly, formation of compound **4** in a refluxing triethyl orthoformate (TEOF) in presence of acetic anhydride was the predominant route. Structures of the isolated derivatives were supported by using the elemental analysis, IR, ^1H - and ^{13}C -NMR as well as their mass spectra (Tables 1 and 2). Although the two derivatives **2** and **3** are quite similar in structure, it is worth mentioning that they displayed NH signals in their ^1H NMR spectra at different positions (10.47 and 8.20 ppm, respectively). The higher downfield shift of the NH signal of **2** could be presumably due to the Cl atom in the attached moiety COCH_2Cl . In addition, all the three compounds **2–4** showed signals around 3.8 ppm due to the OCH_3 attached to the arene ring. Notably, the derivative **4** displayed in addition two more higher field signals at 2.17 and 2.23 ppm due to the OCH_3 groups that substituted to the NH_2 group (Fig. 3). The ^{13}C NMR of compound **3** illustrated interesting features. The spectrum showed two distinct $\text{C}\equiv\text{N}$ groups. The one attached directly to pyridine ring with value like the parent compound (112.7 ppm). The other group, which bonded to the HNCOCH_2 moiety exerted downfield shift and appeared at 126.6 ppm. The carbonyl carbon in that group occurred at 166.9 ppm like that of compound **2**.

The formimidate derivative **5** was obtained by solid fusion of compound **1** with TEOF for a period of 20h (Fig. 3). Structure of **5** was illustrated using spectroscopic and analytical measurements. Compound **5** demonstrated a peak at $m/z = 387$ in its mass spectrum due to the molecular formula. Thus, the spectroscopic finding were compatible with the suggested structure. On the other hand, as shown from Fig. 3, compound **1** reacted with chloroacetic acid in pyridine to give an N-methyl amine derivative (**6**). As declared from Fig. 4, derivative **6** might be occurred via nucleophilic attack of NH_2 group of **1** on the CH_2 group of chloroacetic acid with elimination of one mole of HCl to form the intermediate (A), then followed by decarboxylation^{28,29}. Decarboxylation of the COOH in position 2 of pyridine ring could easily occur due to the high probability to form intramolecular hydrogen bonding between H of the carboxylic group and the lone pair of N atom of pyridine. Notably, the product did not give effervescence with the acidity test confirming the absence of the carboxylic group. Compound **6** displayed a signal at m/z at 345 in its mass spectrum due to the molecular formula. The IR spectrum was devoid from bands due to the $\text{C}=\text{O}$ and OH groups. Instead, it displayed one band due to the NH group (3104 cm^{-1}). On the other hand, the ^1H -NMR spectrum of the **6** exhibited a singlet with integration of three hydrogens ($\delta = 2.78$ ppm) due to the methyl group of the NHCH_3 part. In addition, the spectrum exhibited a signal at 9.75 ppm for the NH proton.

The precursor compound **1** reacted with carbon disulfide to afford the unexpected isothiocyanate pyridine derivative **7**, and not the familiar pyridothiazinethione as we previously reported³⁰. Figure 5 illustrates a proposed pathway for the formation of compound **7**. The last step in the reaction involved the elimination of H_2S gas, which was recognized by its known smell. The mass spectrum of the compound ($m/z = 373$, parent ion peak) as

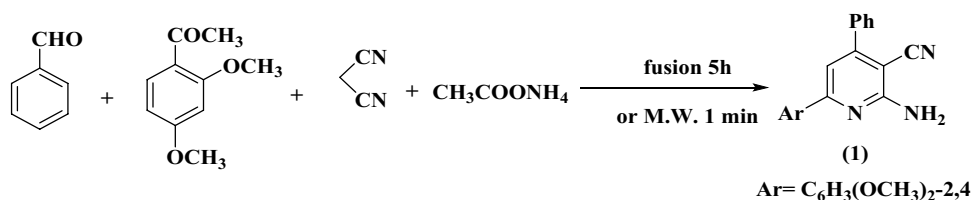


Figure 1. Synthesis of the precursor compound **1**.

Compound	IR data (cm ⁻¹)	NMR data, DMSO- <i>d</i> ₆ δ (ppm)	
		¹ H-NMR	¹³ C-NMR
1	3460 (ν _{NH₂}), 3369 (ν _{NH₂}), 2207 (ν _{CN}), 1602 (ν _{C=N})	3.81 (s, 3H, OCH ₃), 3.88 (s, 3H, OCH ₃), 6.63–8.03 (m, 9H, Ar-H), 7.26 (s, 2H, NH ₂ , exchangeable with D ₂ O)	56.4, 58.6, 109.8, 112.4, 115.4, 126.6, 126.8, 126.9, 127.2, 128.3, 128.8, 129.0, 131.3, 135.6, 138.9, 144.5, 152.9, 155.1, 157.2, 157.9
2	3198 (ν _{NH}), 2225 (ν _{CN}), 1727 (ν _{CO}), 1609 (ν _{C=N})	3.79 (s, 3H, OCH ₃), 3.82 (s, 3H, OCH ₃), 4.19 (s, 2H, COCH ₂ Cl), 6.48–8.01 (m, 9H, Ar-H), 10.47 (s, 1H, NH, exchangeable with D ₂ O)	46.4, 56.3, 58.7, 109.6, 112.7, 116.0, 126.6, 126.8, 126.9, 127.2, 128.3, 128.8, 129.0, 131.2, 135.6, 138.8, 144.4, 152.9, 155.1, 157.2, 157.9, 166.9
3	3174 (ν _{NH}), 2221, 2207 (ν _{CN}), 1726 (ν _{CO}), 1606 (ν _{C=N})	3.84 (s, 2H, COCH ₂ CN), 3.86 (s, 3H, OCH ₃), 3.89 (s, 3H, OCH ₃), 6.69–7.89 (m, 9H, Ar-H), 8.20 (s, 1H, NH, D ₂ O exchangeable)	26.8, 56.3, 58.6, 109.7, 112.7, 116.0, 123.7, 126.6, 126.8, 126.9, 127.2, 128.3, 128.8, 129.0, 131.2, 135.6, 138.8, 144.4, 152.9, 155.1, 157.2, 157.9, 166.9
4	IR (cm ⁻¹): 2221 (ν _{CN}), 1728, 1704 (ν _{CO}), 1606 (ν _{C=N})	2.17 (s, 3H, COCH ₃), 2.23 (s, 3H, COCH ₃), 3.82 (s, 3H, OCH ₃), 3.85 (s, 3H, OCH ₃), 7.13–7.96 (m, 9H, Ar-H)	26.5, 58.6, 60.1, 115.4, 121.2, 121.3, 121.5, 126.3, 126.9, 129.0, 126.1, 129.7, 129.8, 131.3, 131.9, 132.4, 1344, 137.7, 138.0, 152.6, 153.1, 156.8, 157.1, 172.0
5	IR (cm ⁻¹): 2221 (ν _{CN}), 1606 (ν _{C=N})	1.41 (d, 3H, J = 8 Hz, OCH ₂ CH ₃), 3.84 (s, 3H, OCH ₃), 3.87 (s, 3H, OCH ₃), 4.55 (t, 2H, J = 8.6 Hz, OCH ₂ CH ₃), 6.69–9.9 (m, 9H, Ar-H), 8.44 (s, 1H, N=CH)	14.2, 60.2, 60.3, 108.1, 111.7, 120.3, 125.8, 126.1, 128.3, 1286.6, 128.7, 130.0, 131.3, 133.1, 133.7, 135.9, 142.6, 145.4, 152.7, 155.4, 164.2
6	IR (cm ⁻¹): 3104 (ν _{NH}), 2204 (ν _{CN}), 1596 (ν _{C=N})	2.78 (s, 3H, NHCH ₃), 3.79 (s, 3H, OCH ₃), 3.84 (s, 3H, OCH ₃), 7.06–8.11 (m, 9H, Ar-H), 9.75 (s, 1H, NH)	30.2, 56.4, 58.6, 109.8, 112.4, 115.4, 126.6, 126.8, 126.9, 127.2, 128.3, 128.8, 129.0, 131.3, 135.6, 138.9, 144.5, 152.9, 155.1, 157.2, 157.9
7	IR (cm ⁻¹): 2220 (ν _{CN}), 1596, 1571 (ν _{C=N}), 1492 (ν _{C=S})	3.82 (s, 3H, OCH ₃), 3.86 (s, 3H, OCH ₃), 6.70–8.05 (m, 9H, Ar-H)	56.4, 58.6, 108.7, 111.2, 115.3, 126.6, 126.8, 126.9, 127.1, 128.3, 128.6, 129.0, 132.3, 135.6, 138.9, 140.4, 144.5, 151.9, 155.2, 156.8, 157.9
8	IR (cm ⁻¹): 3204 (ν _{NH}), 2223 (ν _{CN}), 1649 (ν _{S=O}), 1605 (ν _{C=N})	2.71 (s, 3H, CH ₃), 3.83 (s, 3H, OCH ₃), 3.87 (s, 3H, OCH ₃), 6.71–7.87 (m, 13H, Ar-H), 10.76 (s, 1H, NH)	21.3, 55.8, 56.1, 85.6, 98.8, 107.1, 111.1, 111.7, 113.7, 114.4, 127.4, 128.3, 129.2, 129.3, 132.6, 137.6, 136.7, 139.0, 154.4, 158.3, 158.4, 160.2, 165.3
9	IR (cm ⁻¹): 2224 (ν _{CN}), 1763, 1723 (ν _{C=O}), 1608 (ν _{C=N})	3.78 (s, 3H, OCH ₃), 3.87 (s, 3H, OCH ₃), 6.64–8.21 (m, 11H, Ar-H)	60.2, 60.3, 111.7, 125.8, 126.1, 128.3, 128.5, 128.7, 130.4, 131.3, 133.1, 133.7, 135.9, 142.7, 145.4, 152.5, 153.0, 157.2, 157.9, 164.5, and 164.9
10	IR (cm ⁻¹): 2224 (ν _{CN}), 1789, 1730 (ν _{C=O}), 1609 (ν _{C=N})	3.81 (s, 3H, OCH ₃), 3.88 (s, 3H, OCH ₃), 6.65–8.23 (m, 13H, Ar-H)	58.3, 58.7, 109.8, 110.8, 111.0, 113.6, 113.8, 116.0, 117.0, 117.9, 119.5, 120.2, 120.4, 123.8, 129.3, 130.4, 130.8, 144.0, 148.5, 148.6, 151.4, 162.5, 162.9
11	IR (cm ⁻¹): 3369 (ν _{NH₂}), 3219 (ν _{NH₂}), 1610 (ν _{C=N})	3.76 (s, 3H, OCH ₃), 3.83 (s, 3H, OCH ₃), 6.56–8.52 (m, 10H, Ar-H), 11.37 (s, 2H, NH ₂)	55.8, 56.1, 98.8, 106.7, 107.1, 114.4, 119.3, 127.4, 129.2, 132.6, 143.5, 150.2, 151.2, 155.0, 157.3, 157.4, 158.4, 160.2
12	IR (cm ⁻¹): 3369 (ν _{NH₂}), 3219 (ν _{NH₂}), 2201 (ν _{CN}), 1610 (ν _{C=N})	3.83 (s, 3H, OCH ₃), 3.87 (s, 3H, OCH ₃), 6.70–8.04 (m, 14H, Ar-H), 10.32 (s, 2H, NH ₂ , D ₂ O Exchangeable)	60.2, 60.3, 125.8, 126.1, 128.3, 128.6, 128.7, 130.4, 131.3, 133.1, 133.7, 135.9, 142.7, 145.4, 164.2, 164.5, 164.9, 168.0, 169.4
13	IR (cm ⁻¹): 3423 (ν _{OH&NH₂} , broad), 2204 (ν _{CN}), 1596 (ν _{C=N})	3.52 (s, 2H, NH ₂ , D ₂ O Exchangeable), 3.86 (s, 3H, OCH ₃), 3.96 (s, 3H, OCH ₃), 6.70–8.04 (m, 9H, Ar-H), 12.58 (s, 1H, OH, D ₂ O Exchangeable)	55.8, 56.1, 85.0, 93.5, 98.8, 107.1, 114.4, 114.8, 119.3, 127.4, 129.2, 132.6, 143.5, 150.2, 152.9, 155.0, 158.4, 158.8, 160.2, 165.8
14	IR (cm ⁻¹): 3460, 3363, 3221 (ν _{NH₂}), 2203 (ν _{CN}), 1616 (ν _{C=N})	3.82 (s, 3H, OCH ₃), 3.86 (s, 3H, OCH ₃), 6.65–8.01 (m, 9H, Ar-H), 7.20 (s, 2H, NH ₂ , D ₂ O exchangeable), 9.28 (s, 2H, NH ₂ , D ₂ O exchangeable)	55.8, 56.1, 77.4, 98.8, 107.1, 114.4, 114.5, 118.4, 119.3, 127.4, 129.2, 132.6, 143.5, 150.2, 155.0, 156.6, 158.4, 160.2, 162.0, 162.2
15	IR (cm ⁻¹): 2991 (ν _{NH}), 1710 (ν _{CO}), 1610 (ν _{C=N})	2.36 (s, 3H, N=CCH ₃), 3.82 (s, 3H, OCH ₃), 3.86 (s, 3H, OCH ₃), 6.70–8.05 (m, 9H, Ar-H), 11.51 (s, 1H, NH, exchangeable with D ₂ O)	21.8, 56.5, 58.6, 112.4, 115.5, 126.6, 126.9, 126.8, 127.3, 128.3, 128.7, 129.0, 131.2, 135.7, 138.9, 144.4, 152.5, 155.2, 157.1, 157.8, 168.9

Table 2. IR and NMR data for the reported compounds.

well as its elemental analysis (Table 1) confirmed the proposed chemical formula. Structure of compound 7 was indicated from the disappearing of the stretching frequency bands of the NH₂ group in its IR spectrum as well as the occurrence of a new strong band specific for thiocarbonyl (C=S) group at 1492 cm⁻¹, along with bands due to the still present C≡N and the new C=N groups (Table 2). The structure of the compound was also confirmed from its ¹H- and ¹³C NMR spectra. The proton NMR spectrum displayed no signals due to the NH group, which would be expected if the pyridothiazinethione was the product. Moreover, the ¹³C NMR spectrum of 7 showed a signal for the C≡N group in the normal range (111.2 ppm) similar to that of the parent compound. In addition, the spectrum displayed a signal at 135.6 ppm due to the carbon atom of the N=C=S moiety³¹.

Compound 1 interacted with *p*-toluene sulfonyl chloride, maleic anhydride, and phthalic anhydride to produce *N*-sulfonamide, 2,5-dioxo pyrrole, and 1,3-dioxoisindoline pyridine derivatives (8–10), respectively (Fig. 6). The structures and molecular formulae of the compounds 8–10 were indicated from their spectroscopic measurements and elemental analysis. The IR spectra of the compounds showed the existence of the C≡N group at its normal range (Table 2). In addition, derivative 8 displayed an asymmetric stretching frequency band at 1649 cm⁻¹ with a shoulder due to the symmetric stretching. It also showed a band due to the NH group at 3204 cm⁻¹. The presence of the NH group in 8 was also confirmed from its ¹H NMR spectrum (10.76 ppm). On the other hand, the IR spectra of the two compounds 9 and 10 displayed strong band at 1723 cm⁻¹ characteristic for the carbonyl groups. The ¹³C NMR spectra of the three derivatives (8–10) illustrated the different carbon signal at their appropriate positions.

The interesting pharmacological properties of naphthyridine derivatives as an antioxidant³², anti-inflammatory³³, and antimicrobial³⁴ reagents have prompted us to attempt to synthesize novel naphthyridine derivatives

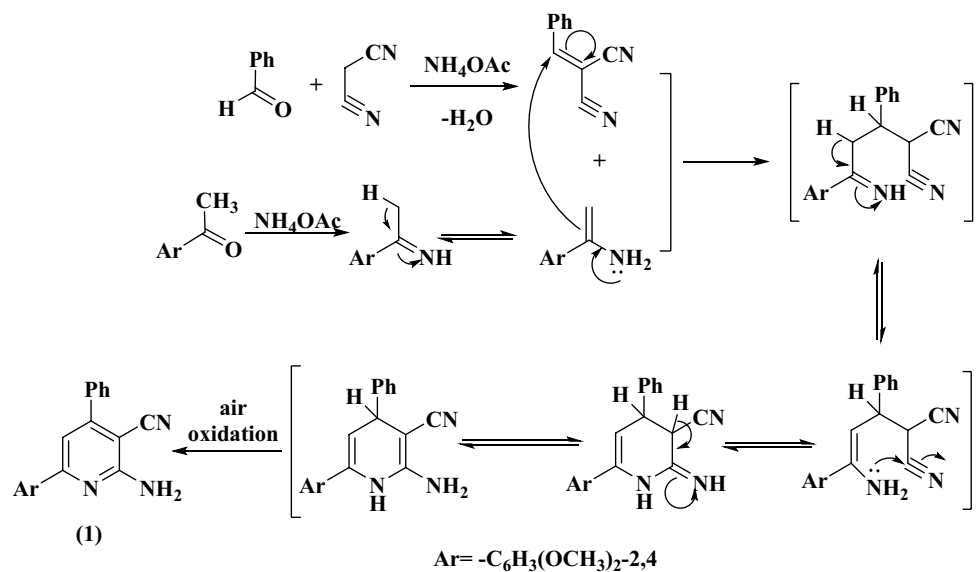


Figure 2. Expected mechanism for formation of compound 1.

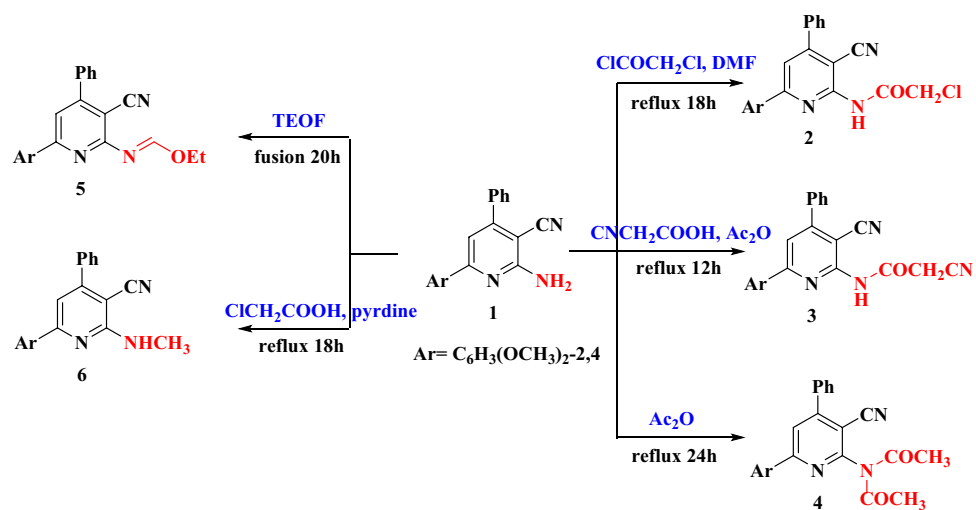


Figure 3. Synthesis and structure of compounds 2–6.

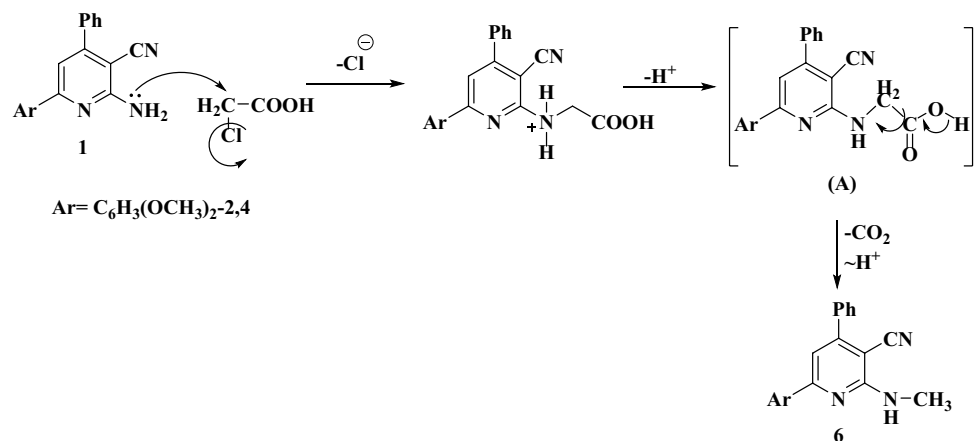


Figure 4. Proposed mechanism for the formation of compound 6.

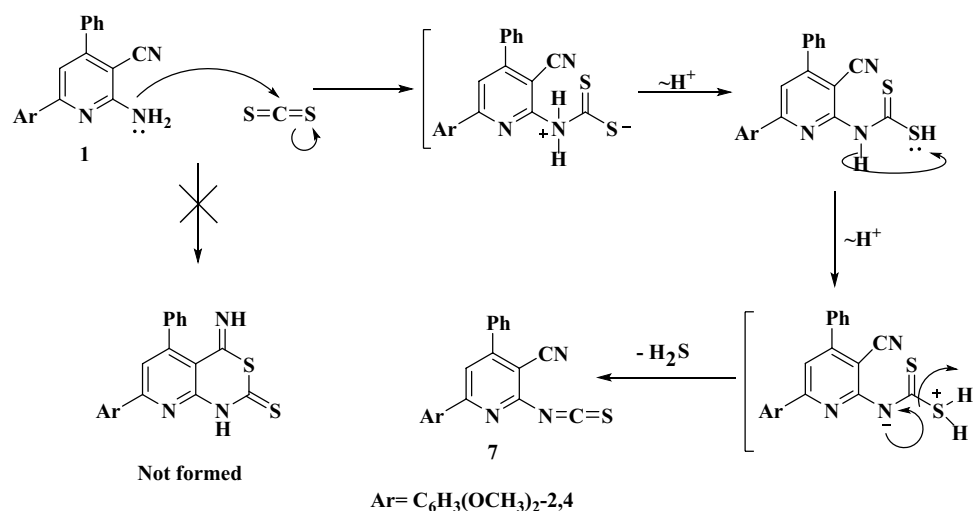


Figure 5. Proposed pathway for formation of compound 7.

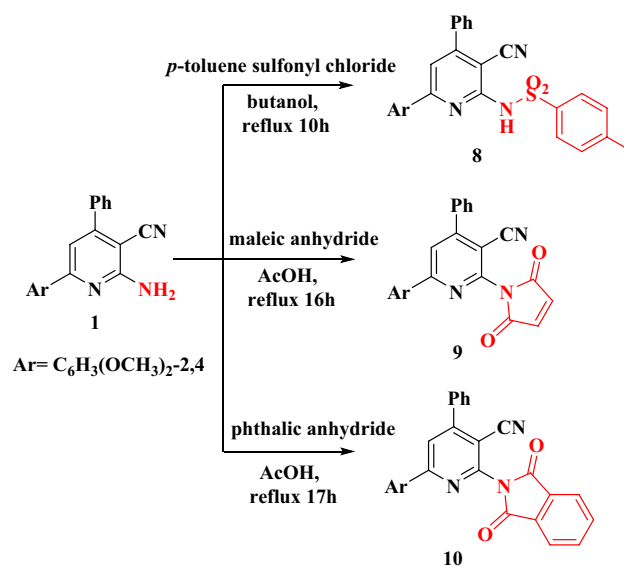


Figure 6. The synthesis and structure of compounds 8–10.

through the reaction of the bifunctional compound **1** with either formamide, benzylidene malononitrile, ethyl cyanoacetate or malononitrile using a catalytic amount of piperidine; reaction of Ac₂O with compound **1** occurred in presence of few drops of H₂SO₄, (compounds **11**–**15**, Fig. 7). The molecular formulae and chemical structure of these new naphthyridine derivatives were elucidated using elemental analyses and spectroscopic data (Table 2). The IR spectrum of the three derivatives **11**–**14** indicated the presence of the NH₂ functional group as they showed asymmetric and symmetric stretching frequencies due to the group (Table 2). The presence of the NH₂ group was further confirmed from the ¹H NMR spectra of the derivatives; NH₂ the signal was disappeared on adding D₂O to the NMR solution (Fig. 8). On the other hand, the existence of OH group in compound **13** and the NH group in compound **15** were also pointed out from their IR and ¹H NMR spectra (Table 2). Moreover, the ¹³C NMR spectra of the four derivatives are consistent with the proposed structures.

Stereochemistry and reactivity descriptors calculations. The energetic optimize geometrical structure parameters, and steric energies of the compound **1** and its derivatives **2**–**8**, **11**, **13** and **15** were computed using hybrid DFT method²⁵. The HOMO and LUMO orbitals in the molecular orbital diagram of a compound explore important information in examining its optical and electric properties as well as the interaction with other entities. Further, the frontier orbitals are responsible for having the different charge transfer (CT) models^{35–37}. The lowest energy minimized stable orientations of the compounds were examined by concentrating on the configuration of the function groups and their orientation relative to each other. The energetically

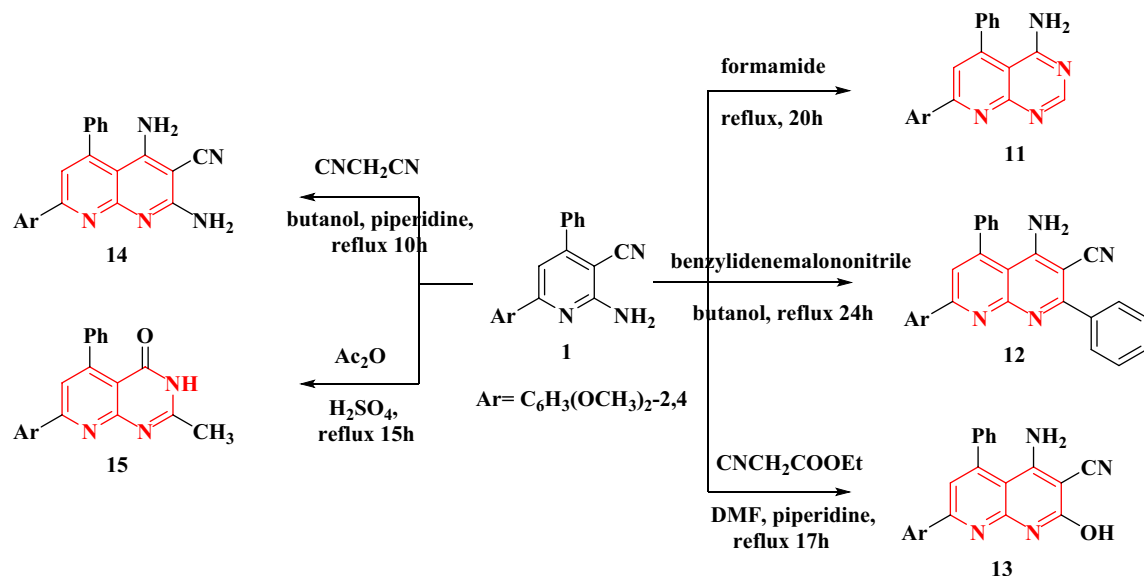


Figure 7. The syntheses and structures of compounds 11–15.

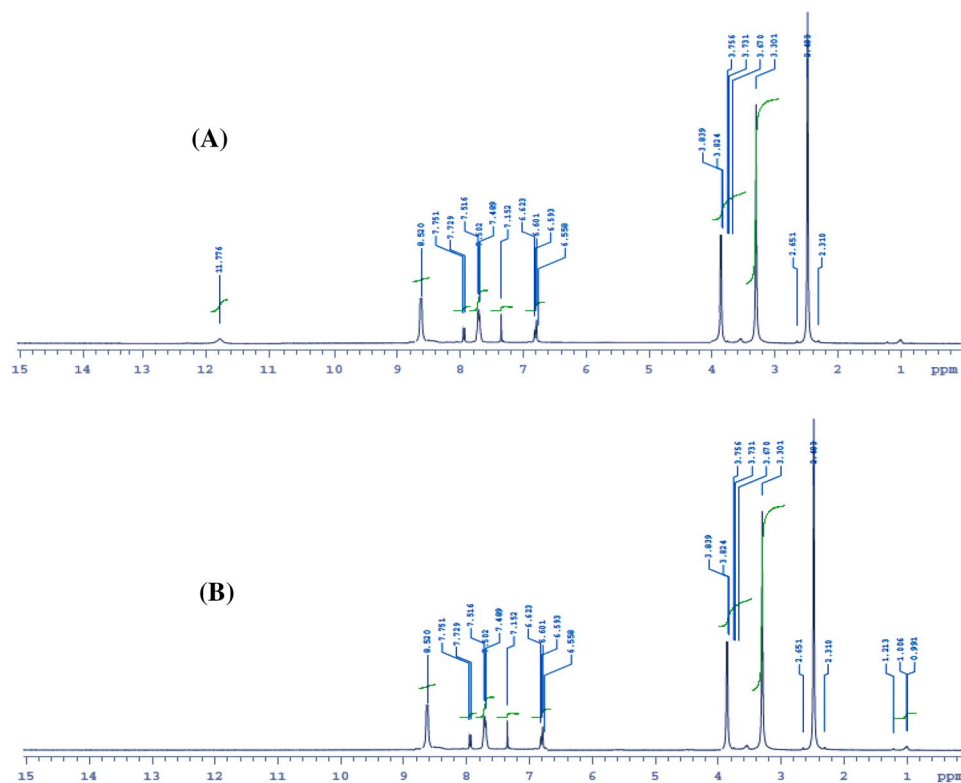


Figure 8. (A) The ¹H-NMR spectrum of 11; (B) The ¹H-NMR spectrum of 11 + D₂O.

minimized structure of compound 1 (43.31 kcal/mol) displayed specified structure features. The molecule was non-planar and unsymmetrical and having a point group of C₁ (Fig. 9). For example, the pyridine ring, amino and cyano groups are lying in one plane, which is forming a dihedral angle = 43.0° with the phenyl ring attached at the fourth site of pyridine cycle. Interestingly, the two hydrogens of the –NH₂ group were directed towards the nitrogen atoms of pyridine ring and cyano group forming some sort of hydrogen bonding with van der Waal displacement equals 2.46 Å (N3–H28) and 2.82 Å (H27–N25), respectively (Fig. 9). The of bond lengths and angles were in normal values^{38–40}. The charge allocation on the different atoms of 1 calculated by Mullikan method is illustrated in Fig. 9B. According to the charge distribution shown, the nitrogen of the amino group (N8) displayed highest negative charge density (–0.76), while nitrogen atoms of pyridine (N3) and cyano moiety (N25) have lower values (–0.51 and –0.24, respectively). Furthermore, the electrostatic potential (ESP) map of

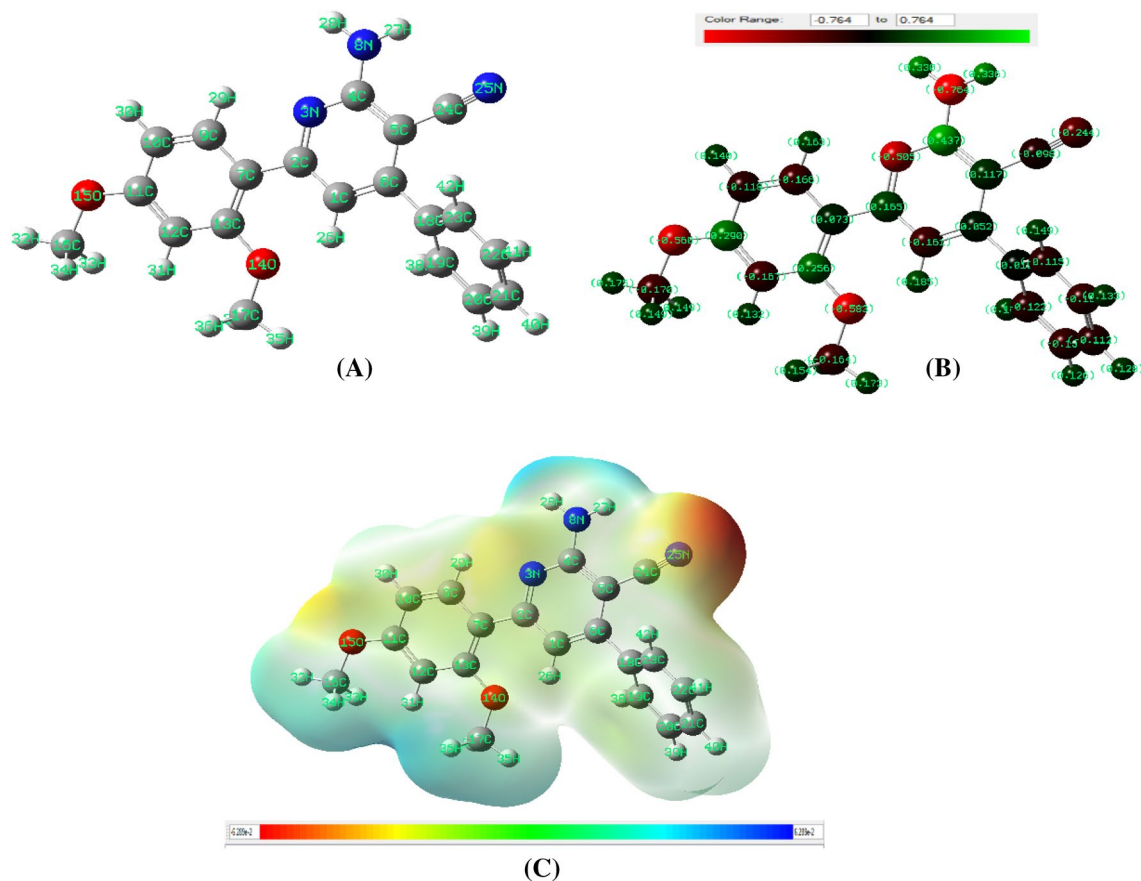


Figure 9. (A) The optimized geometrical structure of compound **1**; (B) The charge distribution on atoms; (C) Molecular electrostatic potential map.

derivative **1** (Fig. 9C) gives important information about the charge distributions of the compound. It distinguishes the reactive sites of the tested compound by showing both the electrophilic and/or the nucleophilic attack regions. In addition, the electrostatic potential map is an effective representation in biological sciences fields³⁸. It determines the positive (shown as a blue color) and negative (appeared as a red color) charged electrostatic potential in the derivative. The color scale of **1** ranged from -0.06289 Hartree (-165.12 kJ/mol) to $+0.06289$ Hartree ($+165.12$ kJ/mol). High negative potential red zones indicated the electrophilic attack sites, while high positive potential blue sections designated appropriate centers for nucleophilic attack. It is well known that derivatives of 2-amino-3-cyanopyridine are polyfunctional compounds that possess properties for susceptible electrophilic and nucleophilic reactions. The perfect nucleophilic location in these derivatives is the NH_2 , while the carbon atom of the cyano group is liable to the electrophilic attack. Thus, several heterocyclic moieties with variable ring sizes like pyrrole, pyridine, pyrimidine and oxadiazine were designed and synthesized using these chemical properties¹³.

The geometrically optimized structural arrangements of compounds **2–5** (Fig. 10) possessed steric minimum energies = 46.93, 46.09, 85.19 and 56.10 kcal/mol, respectively. The structures are unsymmetrical and non-planar (C_1 point group). The non-planarity characteristics are stemmed from the dihedral angle values occurred between the plane of pyridine cycle and the two phenyl parts. All the dihedral angles are found in the range 44° and 45° , respectively. Also, all the bond distances and bond angles have similar values as shown in compound **1**. On the other hand, the pyridine nitrogen performed intramolecular hydrogen bonding with the adjacent hydrogens of the substituents in position two (2: $\text{N3-H47} = 2.35$ Å; 3: $\text{N3-H48} = 2.30$ Å; 4: $\text{N3-H49} = 2.56$ Å; 5: $\text{N3-H39} = 2.44$ Å), Fig. 10. The presence of these hydrogen bonding was also indicated from the broadening of protons signals in $^1\text{H-NMR}$ spectra of molecules.

Energetically optimized configurations of compounds **6–8** (minimum energies are 48.55, 46.34 and 228.17 kcal/mol, respectively) showed non-planar arrangements of the compounds, Fig. 11. Compound **8** showed high steric minimum energy may be due to the presence of the Ar-SO_2 moiety. The planes containing the pyridine ring and the other phenyl parts in the compounds formed dihedral angles in the ranges of 40° – 50° . In the case of compound **6**, the NH group attached to the position 2 of pyridine is lying approximately in the same plane with the pyridine ring itself (dihedral angle of $\text{N3-C4-N21-H36} = 178.8^\circ$). In addition, the proton of the NH made intramolecular H-bonding with the pyridine nitrogen (N3-H36) with a distance equal to 2.29 Å, and consistent with the spectroscopic data. The optimized structure compound **7**, showed that the N=C=S group was linear and formed a bent angle with the pyridine plane ($\text{N3-C4-N9} = 116.99^\circ$), which deviated from the angle 120° characteristic for sp^2 hybridization. No hydrogen bonding was detected in the structure of **7**. However, the other

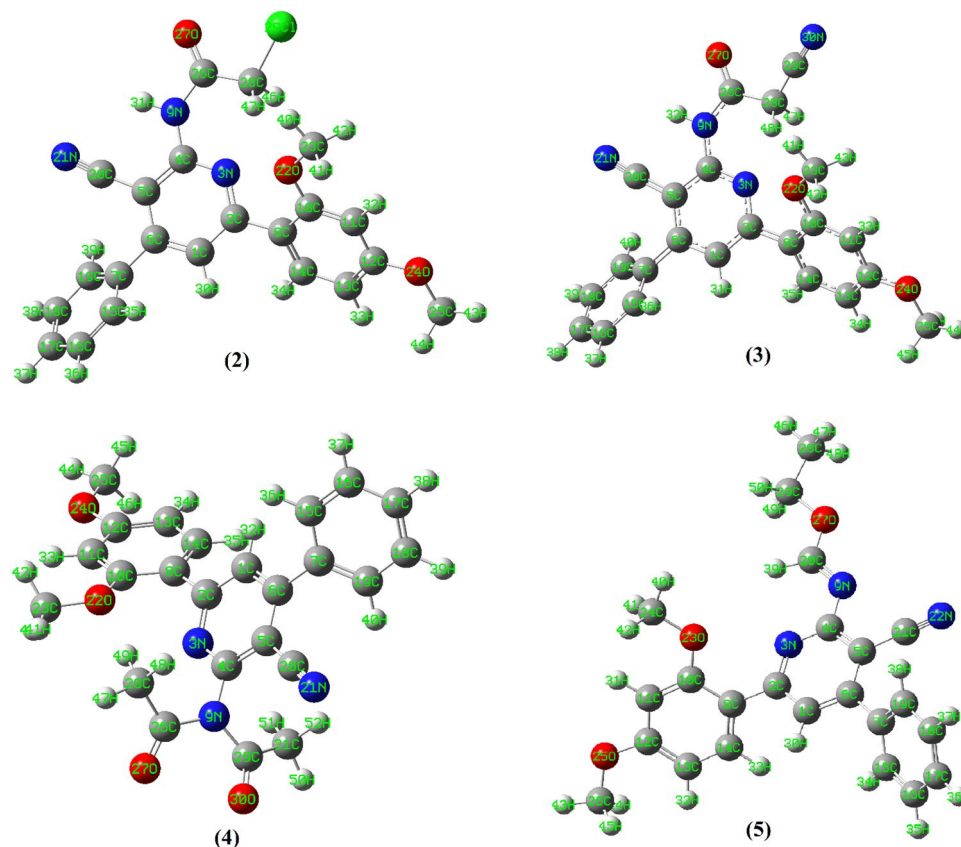


Figure 10. Geometrically optimized structures of compounds 2–5.

values of bond lengths and angles were found to be normal^{38–40}. The energy optimized structure of compound **8** showed that sulfur atom (S33) of HN–SO₂ group (Fig. 11) existed in a distorted tetrahedral arrangement. The bond angles involved in this tetrahedral such as O34–S33–O35 and N9–S33–O35 were 119.6° and 110.3°, respectively. In contradictory to compound **6**, this structure arrangement forced the proton of the NH group to be away from the pyridine nitrogen. However, this proton acquired hydrogen bonding with the nitrogen of the cyano group (H37–N28 = 2.80 Å).

The geometrically optimized configurations of the synthesized naphthyridine derivatives **11**, **13** and **15** are shown in Fig. 12. The minimization energies of the three compounds were 57.39, 59.60 and 50.33 kcal/mol, respectively. The optimized structure of **11** showed that it has unsymmetrical and non-planar geometry. The pyrido-pyrimidine, dimethoxy phenyl and amino groups were planar and lying in one plane, which made a dihedral angle (C1–C6–C7–C14) = 68.3° with the other phenyl ring. On the other hand, one of the amino protons made H-bonding with adjacent nitrogen of pyrimidine part (N21–H39 = 2.39 Å). For compound **13**, energetically optimized geometry showed that it was non-planar. The naphthyridine ring along with the amino, hydroxy and cyano groups exist in one plane and forming with both dimethoxy phenyl and the other phenyl groups dihedral angles with the values of 177.4° and 44.4°, respectively. On the other hand, the OH proton was directed towards the nitrogen atom of the cyano group (N30–H42) with van der Waals separation of 2.86 Å. One of the amino protons is also directed to the cyano group (N30–H41) with a distance equal to 2.88 Å. The optimized structure of compound **1** showed that the pyrido pyrimidinone moiety and the phenyl group of the dimethoxy phenyl part are planar. The other phenyl group exerted a dihedral angle with a value of 57.9° with that plane. The calculated structure displayed some sort of hydrogen bonding interaction between one of the nitrogen atoms of pyrimidinone ring and a hydrogen atom of adjacent –CH₃ group (N19–H40 = 2.52 Å). Also, the carbonyl oxygen interacted with the adjacent NH proton (O23–H38) with a bond length of 2.43 Å. Further, the methoxy oxygen made H-bond interaction with the adjacent hydrogen of the pyrido group (O25–H29) with a value of 2.07 Å.

The chemical reactivity parameters such as the frontier *HOMO* and *LUMO* orbitals, energy differences gaps (ΔE), chemical potentials (V), ionization potentials (I), electronegativity (X) values, electron affinities (A), chemical softness (S) and hardness (η) values, as well as electrophilicity index (ω) amounts of the reported compounds are tabulated in Table 3^{41,42}. Total energies, dipole moments (DM) and binding energies (BE) are also given. The DFT (B3LYP) calculations were performed to estimate the energies of the frontier molecular orbitals. The energy of the *HOMO* orbital describes the donation ability of the electrons and the energy of *LUMO* orbital refers to the withdraw capability of electrons. The difference in energies between the *HOMO* and *LUMO* (ΔE) points out to the molecular stability that demonstrates important parameters for the evaluation of the properties of electrical transport. The small differences in energy declare the facility of charge transfer (CT) as well as polarization in

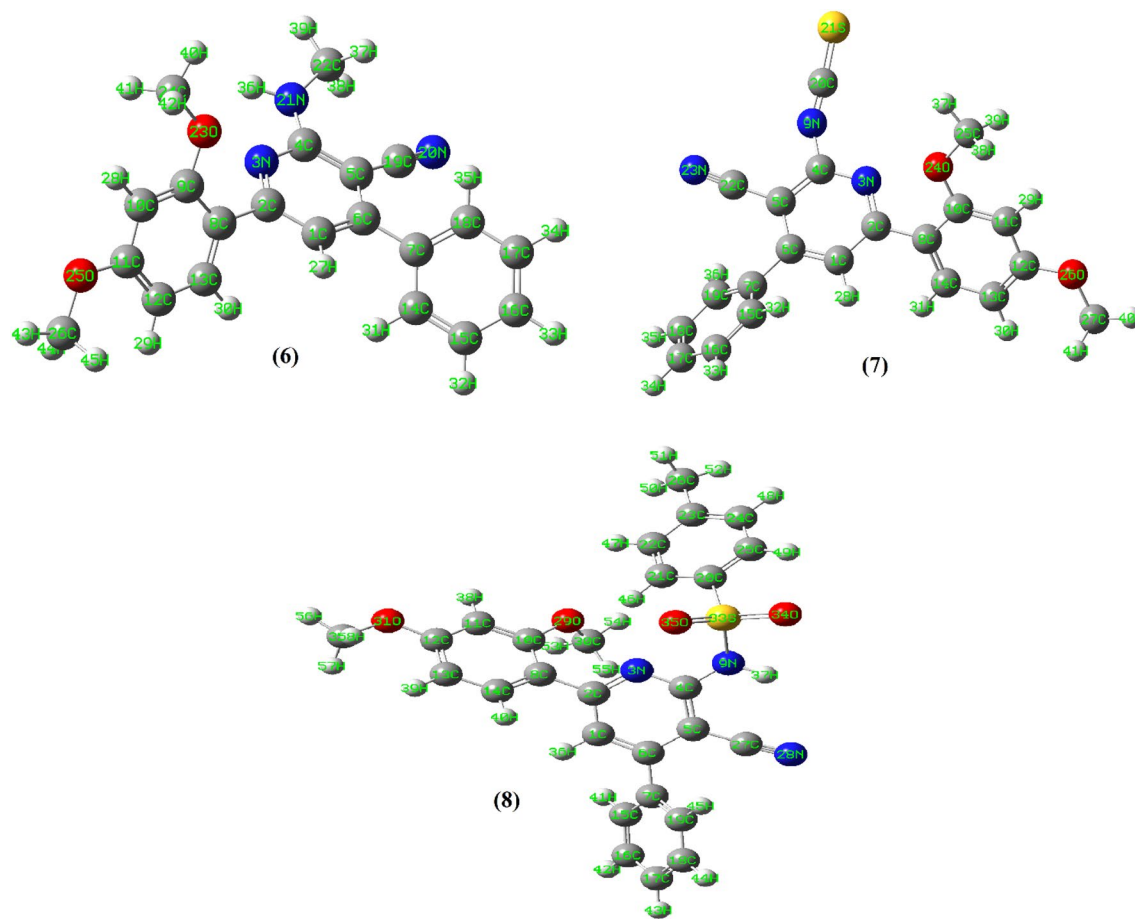


Figure 11. Geometrical optimize structures of compounds 6–8.

the compounds^{36,38}. Derivative **13** had the smallest ΔE value. Moreover, the electronegativity factors reflect the electrostatic potentials, which show the partial transfer of the electron from a lowest electronegative to another highest electronegative part. The diminishing in electronegativities of the derivatives had the order: $3 > 4 > 2 > 8 > 7 > 13 > 5 > 11 > 15 > 1 > 6$. On the other side, results of small amounts of chemical hardness for the molecules reflected the capability of charge transfer within these compounds. The order of increasing charge transfer inside the molecules was: $5 < 6 \approx 8 < 2 \approx 3 \approx 11 \approx 15 < 4 < 7 < 1 < 13$. The binding energy (BE) represents the smallest amount of energy that required to disassemble a molecule into its constituent atoms. The values of binding energies can be calculated from the empirical relation⁴³:

$$BE = \frac{[aE_C + bE_H + cE_N + dE_O + eE_S + fE_{Cl}] - [E_{compound}]}{a + b + c + d + e + f}$$

a , b , c , d , e and f are the numbers of carbon, hydrogen, nitrogen, oxygen, sulfur or chloride in molecules. The E_C , E_H , E_N , E_O , E_S and E_{Cl} values represent the total energies of ground state for the different atoms. The $E_{compound}$ exemplifies the energies of minimized structures of the calculated compounds. According to Table 3, order of decreasing BE of compounds was: $11 > 6 > 4 \approx 5 > 3 > 15 \approx 1 > 13 > 2 > 7 > 8$.

Biological activity studies. *The antimicrobial activities.* Results of antimicrobial activities of screened compounds **1–8**, **11**, **13** and **15** showed that they have diverse antibacterial activities with respect to the standard Cefoperazone that varied according to the screened microbial strain and the tested compound (Tables 4 and 5). The investigated compounds displayed, with different ranges, abilities to inhibit the metabolic development of the screened bacteria and pointed out that they possess wide-spectrum properties. The various structures and substituents of the tested compounds obviously functioned an important role and considered the key pillar for their biological activity (vide infra). The activity of the reported compounds might be attributed to the existence of NH_2 , NH , OH , $C=O$ and $C\equiv N$ functional moieties. It was suggested that the mode of action of compounds is the formation of H-bond interaction between these groups and active places of cell constitutes along with interference with normal cell^{43–45}. The cell membranes consist of permeable lipid layers, which allow the passage of soluble lipid materials. Therefore, the lipophilicity characteristics play a vital parameter that affects inhibition of bacteria. Thus, increasing the lipophilicity might enhance inhibition ability of screened compound. On the other hand, the tested compounds exhibited completely different trend for the antifungal activity studies. Except

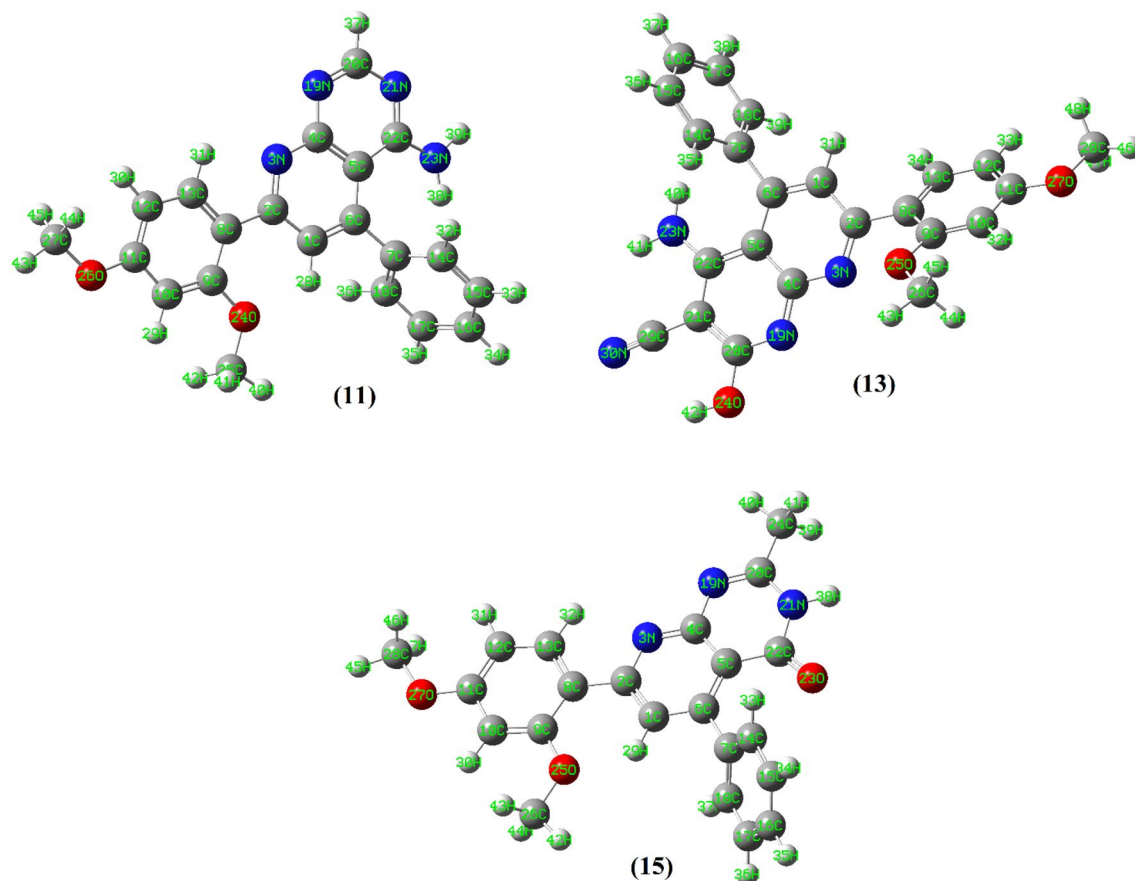


Figure 12. Geometrically optimized structures of compounds 11, 13 and 15.

Parameter	1	2	3	4	5	6	7	8	11	13	15
Total Energy (au)	-1086.8	-1698.9	-1331.6	-1391.9	-1278.6	-1126.0	-1521.8	-1905.4	-1180.2	-1331.6	-1239.4
DM (Debye)	6.80	11.30	12.47	12.56	8.45	4.80	8.99	9.67	6.30	8.47	2.33
HOMO (eV)	-5.56	-6.22	-6.28	-6.23	-5.88	-5.58	-6.07	-6.24	-5.72	-5.77	-5.70
LUMO (eV)	-1.61	-2.16	-2.23	-2.20	-1.54	-1.40	-2.07	-2.05	-1.66	-1.90	-1.64
ΔE (eV)	3.95	4.06	4.06	4.03	4.34	4.18	4.00	4.19	4.06	3.87	4.06
X (eV)	3.58	4.19	4.25	4.21	3.71	3.49	4.07	4.14	3.69	3.83	3.67
V (eV)	-3.58	-4.19	-4.25	-4.21	-3.71	-3.49	-4.07	-4.14	-3.69	-3.83	-3.67
A (eV)	1.61	2.16	2.23	2.20	1.54	1.40	2.07	2.05	1.66	1.90	1.64
I (eV)	5.56	6.22	6.28	6.23	5.88	5.58	6.07	6.24	5.72	5.77	5.70
η (eV)	1.98	2.03	2.03	2.01	2.17	2.09	2.00	2.09	2.03	1.94	2.03
S (eV)	0.99	1.02	1.01	1.01	1.08	1.05	1.00	1.05	1.02	0.97	1.02
ω (eV)	3.25	4.31	4.46	4.41	3.17	2.92	4.14	4.10	3.35	3.79	3.32
BE (kcal/mol)	262.15	260.53	262.22	261.64	262.63	262.68	258.42	257.57	263.31	261.93	262.17

Table 3. The global chemical reactivity descriptors for the investigated compounds.

for the two compounds 2 and 9, all the other screened compounds were inactive against *A. flavus*, *A. niger* and *F. oxysporum*. Compound 2 showed a satisfactory antifungal activity against *A. niger* (inhibition zone = 10 mm), while compound 9 showed the highest active towards *F. oxysporum* (inhibition zone = 15 mm).

DPPH radical scavenging assay. Normal physiology of living organisms is usually engaged with free radicals. Excessive amount of free radicals along with reactive oxygen are responsible for the induction of cellular oxidative damage. This damage in the cells would result in varieties of chronic diseases like for example arteriosclerosis, cancer, inflammatory disorders, and geriatric disorder⁴⁶. The free radical agent 2,2-Diphenyl-1-picrylhydrazyl (DPPH) is widely used to estimate scavenging ability of various samples. Its significant decrease is dependent on the exposition to scavengers with proton radicals⁴⁷. Thus, scavenging of the stable DPPH radical is valuable

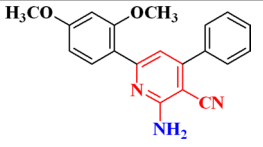
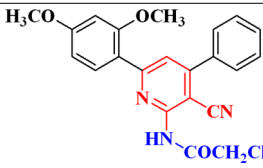
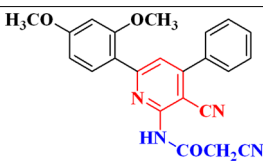
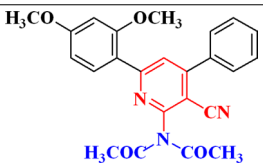
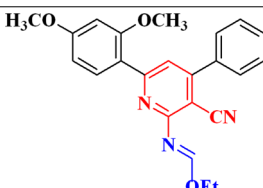
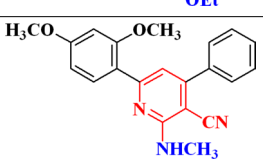
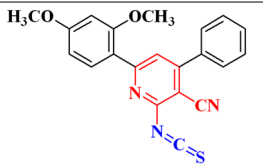
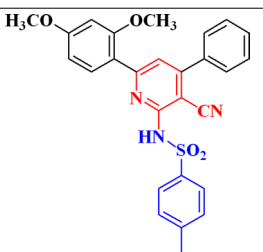
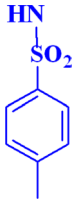
No	Structure		Antibacterial activity (inhibition zone, mm)				
	Compound	Fragment	Gram +ve bacteria		Gram -ve bacteria		
			<i>S. aureus</i>	<i>B. cereus</i>	<i>E. coli</i>	<i>S. typhimurum</i>	<i>Y. enterocolitica</i>
	Cefoperazone	–	12	12	15	11	12
1		NH_2	–	–	–	10	–
2		$\text{HN-COCH}_2\text{Cl}$	–	–	–	9	10
3		$\text{HN-COCH}_2\text{CN}$	–	–	12	9	12
4		$\text{H}_3\text{COC-N-COCH}_3$	–	–	–	12	9
5		N=OEt	15	–	9	15	–
6		NHCH_3	18	–	10	–	13
7		N=C=S	–	9	8	10	–
8			–	9	–	12	–

Table 4. Correlation between the antibacterial activities and the structures of compounds 1–8.

in determining antioxidant activity of a compound in a relatively short period. DPPH radical is little affected by side reactions like metal chelation and enzyme inhibition. This might be due to the extensive delocalization of its unpaired electron⁴⁸. A stable diamagnetic radical is formed when the DPPH neutralize by an electron or a

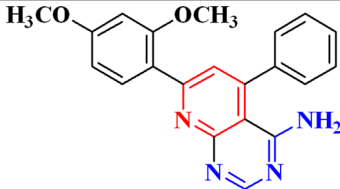
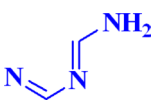
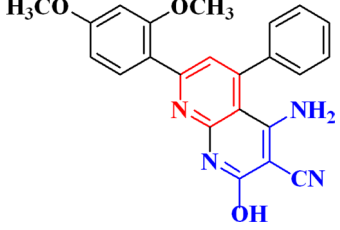

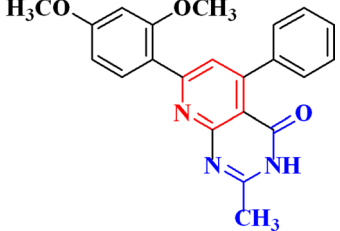
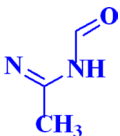
No	Structure		Antibacterial activity (inhibition zone, mm)				
	Compound	Fragment	Gram +ve bacteria		Gram -ve bacteria		
			<i>S. aureus</i>	<i>B. cereus</i>	<i>E. coli</i>	<i>S. typhmirus</i>	<i>Y. enterocolitica</i>
	Cefoperazone	–	12	12	15	11	12
11			–	14	12	13	–
13			–	13	10	13	–
15			–	9	–	10	10

Table 5. Correlation between the antibacterial activities and the structures of compounds 11, 13 and 15.

hydrogen²⁶. DPPH gives deep violet color and displays a strong absorption band in the visible region ($\lambda_{\max} = 517$ nm) corresponding to its unpaired electron. In presence of scavenging reagent, the electron paired up, absorption diminishes, and color turns to yellow. The decolorization is a stoichiometric step and it is relative to the number of electrons picked up. This reduction capability of DPPH radicals is induced by antioxidant agents and is estimated by lowering the absorbance of λ_{\max} at 517 nm⁴⁹. Figure 13 displays the DPPH radical scavenging activities of the investigated compounds (1–15). The commercial phenolic antioxidant, butylated hydroxyanisole (BHA) was used as a standard. As can be seen from Fig. 13, scavenging of DPPH radicals are dependent on concentration of the synthesized compounds. At 100 $\mu\text{g/ml}$, the two compounds (5 and 12) exhibited the lowest antioxidant activity, while compound 8 gave the highest scavenging activity (IC_{50} 43.39 $\mu\text{g/ml}$) against the DPPH radical. The obtained scavenging activity was raised by increasing the compounds concentrations ranged from 12.5 to 100 $\mu\text{g/ml}$. This increasing in scavenging activity is harmonized with the decrease in the DPPH radical concentration. It also indicated the reducing ability of DPPH radical by potential antioxidant properties of the reported compounds.

Structure–activity relationship. Results of this study declared the existence of relations between the antimicrobial actions of the reported derivatives and the different types of the substituents bonded to the enamino-nitrile pyridine derivatives. It is worth mentioning that the substitutions varieties and the structure diversity of the tested compounds played an outstanding role in their biological activities. From the reactivity descriptors (Table 3), the data of antibacterial activity (Tables 4 and 5) and the antioxidant studies (Fig. 13), correlation between the structures and activities of the reported molecules can be achieved. The structure arrangement of a molecule is a reflection of its activity, i.e., analogous compounds could have similar activities. This fact is the central backbone of structure–activity relationship (SAR) proposition. The SAR concept thus supposes that structural characteristics of a molecule, such as its geometric and electronic properties have features responsible for its chemical, physical, and biological features. So, the SAR can be employed to speculate the biological activity of a compound from its structure arrangements and its substituents. Now, this approach is commonly applied in drug design and drug discovery to guide the development of the desired new compounds. As can be seen from Table 4, compound 1 showed antibacterial activity towards the Gram-negative bacteria *S. typhmirus* with inhibition activity zone = 10 mm. On substitution of NH_2 of 1 by the $\text{HN-COCH}_2\text{Cl}$ moiety to yield compound 2, the antibacterial activity against the Gram-negative bacteria enhanced and showed in hibition activity toward to the bacteria strains (*S. typhmirus* and *Y. enterocolitica*). Further, replacement of the fragment $\text{HN-COCH}_2\text{C}\equiv\text{N}$ to give compound 3, i.e., $\text{C}\equiv\text{N}$ instead of Cl in compound 2, more enhancement in its antibacterial activity against the Gram-negative bacteria was indicated. Obviously, these fragments increased the lipophilic properties

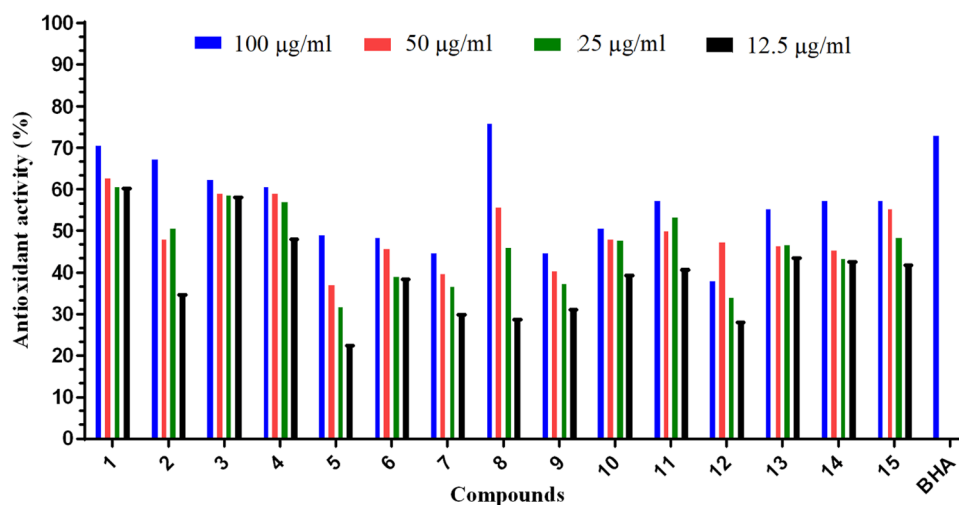


Figure 13. The DPPH radical scavenging activity of the reported compounds (1–15). Values are expressed as mean ($n=3$) of the percent inhibition of the absorbance of DPPH radicals.

with the order $1 < 2 < 3$. Interestingly, this was the order of the calculated electrophilicity index, chemical potential, and chemical softness of the three derivatives (Table 3). In the case of compound 4, the substituted branched group, $N(\text{COCH}_3)_2$, instead of NH_2 caused inhibition disability and reduced its antibacterial activity. On the other hand, replacement of the NH_2 group of compound 1 by the fragments $\text{N}=\text{OEt}$, NHCH_3 and $\text{N}=\text{C}=\text{S}$ to give the compounds 5–7, enhanced the antibacterial ability of the compound against the Gram-positive bacteria with high inhibition zones (Table 4). These data are also correlated with the reactivity descriptors of these derivatives (Table 3) as well as antioxidant activities (Fig. 13). The interaction between inhibitors, such as synthetic compounds and bacteria could be due to either diffusion or cell permeability. Thus, the cell wall of a bacteria plays crucial role against the screened inhibitor. The cell wall of the Gram-positive bacteria mainly consisted of multiple layers of peptidoglycan that forms a thick (cell wall = 20–30 nm) and rigid membrane structure, while the cell wall of the Gram-negative bacteria has an outer membrane and fewer layers of peptidoglycan (cell wall is 8–12 nm thick)⁵⁰.

Reactions of compound 1 with formamide, $\text{N}\equiv\text{C}-\text{CH}_2-\text{COOEt}$ and $\text{Ac}_2\text{O} + \text{H}_2\text{SO}_4$ gave different category of products (naphthyridine derivatives 11, 13 and 15 (Table 5). The reported naphthyridine derivatives were expected to have important biological applications^{32–34}. These interesting cyclic products showed fair antibacterial inhibition with comparable activities towards the Gram-negative bacteria and one of the Gram-positive bacteria (*B. cereus*). They also have almost analogous antioxidant activities (Fig. 13). Interestingly, the reported compounds (11, 13 and 15) have also comparable calculated reactivity descriptors (electrophilicity index, chemical potential and chemical softness, Table 3).

Molecular docking studies. Computation of molecular docking is a superior rout to estimate the interaction between small, prepared molecules and macromolecular biological targets⁵¹. Analyses of the docking data are commonly utilized in detecting the conformation variations that associated with the binding sites of macromolecular receptors, like nucleic acid, to host the docked hydrophobic inhibitor. Molecular docking analysis of the compounds 1–8, 11, 13 and 15 were executed by using MOE program. The investigation intended to declare the types of interactions between the tested compounds and DNA as well as to distinguish between the possible binding poses and energy values. The conformations possibilities of the docked compound and a B-nucleic acid (PDB ID:1BNA) were valued from the binding scores, hydrophobic interactions, and different types of hydrogen bond formation. Molecular docking studies estimate the way to how docked molecules are fundamentally adjusted into the minor groove of the DNA and declare the type of interactions (binding poses) with the DNA bases, which could be either hydrophobic, ionic or hydrogen bonding (Figs. 14, 15 and 16). These binding cases are evaluated using the mathematical scoring function (S)²³. These score functions values are usually negative. The large negative values of S imply that the docked compound has high binding affinity to bind with the macromolecular receptor. Notably, molecular docking analysis of the investigated derivatives displayed high negative values for the functions binding scores and confirmed the good efficiencies of these bioactive molecules towards the investigated target. Table 6 tabulates the computed docking findings (score and rmsd values, types and energies of interactions). As can be observed from Figs. 14, 15 and 16 and Table 6, the nucleotide regions DG, DC, and DA of the DNA receptor were the most optimum docking zones. Binding modes and poses were due to hydrophobic interactions between nucleotides residues like DA, DC, and DG and aromatic parts of the compounds. Further, hydrogen-donor, hydrogen-acceptor and/or π -H occurred between compounds and DNA parts were another modes of interactions. The binding interaction was found to have the order: $3 < 8 < 15 < 7 < 6 < 4 < 2 < 11 < 13 < 5 < 1$.

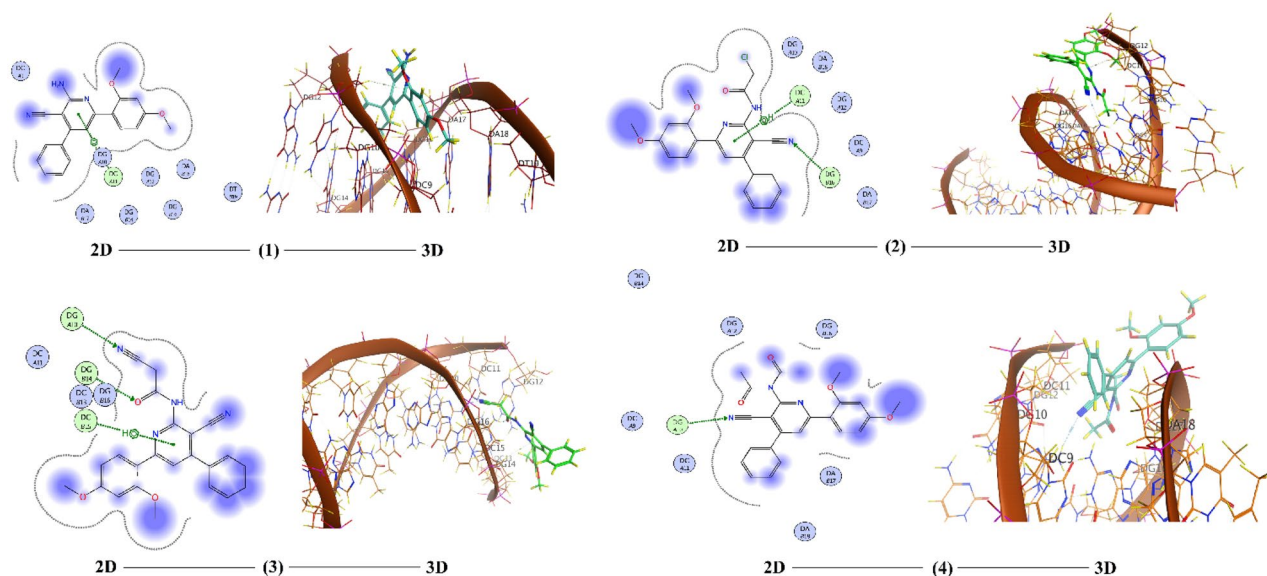


Figure 14. The 2D and the 3D representations of the interaction of investigated compounds 1–4 with DNA.

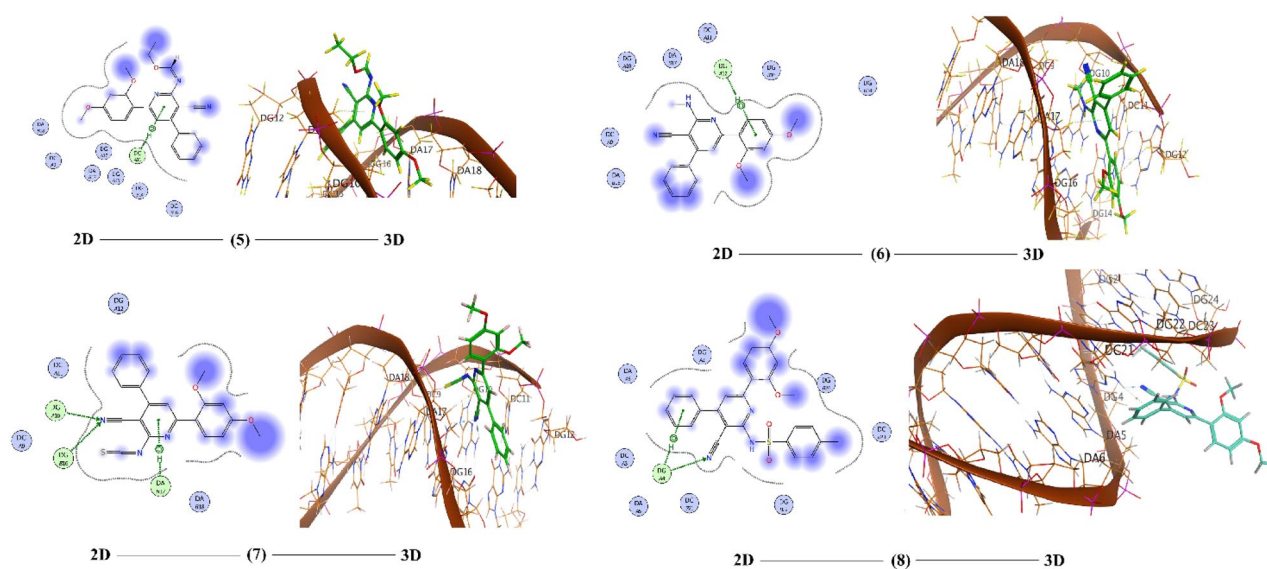


Figure 15. The 2D and the 3D representations of the interaction of investigated compounds 5–8 with DNA.

Conclusion

Green syntheses of fourteen molecularly designed pyridine derivatives were performed from the reactions of the enaminonitrile 2-amino-6-(2,4-dimethoxyphenyl)-4-phenylnicotinonitrile with some selected reagents. The density functional theory calculations for some selected compounds and their computed quantum global reactivity descriptors showed their interesting structural arrangements and their possible biological activities. The antimicrobial inhibition of the molecules that screened against four bacterial strains as well as their antioxidant activities indicated their potency as potential antibiotic reagents. The structure–activity relationships of these compounds were also correlated with the data of antibacterial and antioxidant activities. Furthermore, the molecular docking studies for some derivatives with a B-DNA nucleic acid (PDB ID:1BNA) illustrated high negative binding scores due to the presence of different hydrogen bonding interactions (H-acceptor, H-donor and π -H). Such interactions reflected their high binding affinities to the tested macromolecular receptor.

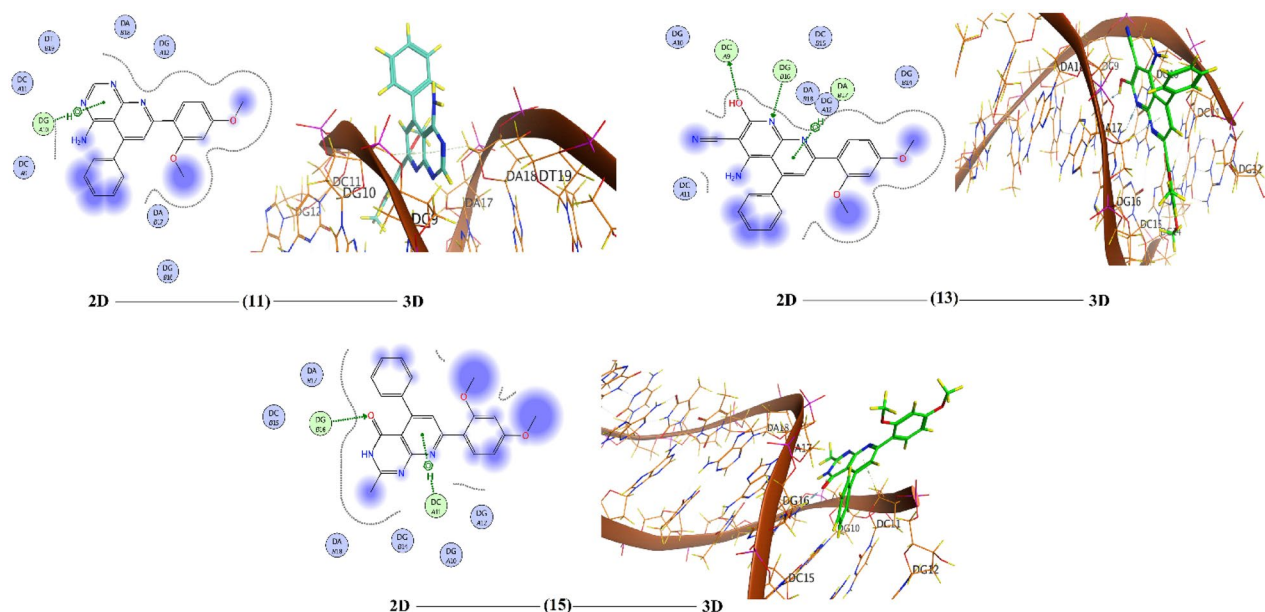


Figure 16. The 2D and the 3D representations of the interaction of investigated compounds **11**, **13** and **15** with DNA.

Compound	S (kcal/mol)	rmsd value ^a	Ligand-Receptor	Interaction type	Interaction distance, Å	E (kcal/mol)
1	-8.54	1.50	6-ring-C4' (DC 11A)	π -H	3.79	-0.6
2	-6.79	1.86	N31-N2 (DG 16B)	H-acceptor	3.49	-1.5
			6-ring-C4' (DC 11A)	π -H	4.03	-0.6
3	-4.66	1.32	O43-N2 (DG 14 B)	H-acceptor	3.15	-2.0
			N48-N2 (DG 10 A)	H-acceptor	3.19	-1.0
			6-ring-C4' (DC 15 B)	π -H	4.44	-1.2
4	-6.56	1.41	N30-N2 (DG 10 A)	H-acceptor	3.34	-2.9
5	-8.19	2.36	6-ring-C4' (DC 11 A)	π -H	3.85	-0.9
6	-6.50	2.01	6-ring-C5' (DG 12 A)	π -H	4.44	-0.6
7	-6.46	2.37	N32-N2 (DG 10 A)	H-acceptor	3.13	-3.7
			N32-N2 (DG 16 B)	H-acceptor	3.18	-1.5
			6-ring-C4' (DA 17 B)	π -H	3.82	-0.8
8	-5.23	1.69	N45-N2 (DG 4 A)	H-acceptor	3.19	-0.8
			6-ring-N2 (DG 4 A)	π -H	4.13	-0.7
11	-7.24	1.46	6-ring-C5' (DG 10 A)	π -H	3.55	-1.1
13	-8.01	1.55	O35-O2 (DC 9 A)	H-donor	3.01	-2.1
			N28-N2 (DG 16 B)	H-acceptor	3.11	-3.2
			6-ring-C4' (DA 17 B)	π -H	3.69	-0.7
15	-6.25	1.40	O33-N2 (DG 16 B)	H-acceptor	2.98	-4.1
			6-ring-C4' (DC 11 A)	π -H	3.70	-1.0

Table 6. The molecular docking data of the reported compounds. ^aThe root mean square deviation; a measure of the average distance between the docked atoms.

Data availability

Any datasets used that support the findings of this study are available from the corresponding author upon reasonable request. A supplementary file, containing the figures of ¹H- and ¹³C-NMR of compound **1** and a table of the % yields of all products, is provided.

Received: 31 March 2023; Accepted: 13 September 2023

Published online: 20 September 2023

References

- Farag, A. A., Mohamed, E. A., Anwer, K. E., Azmy, E. A. & Sayed, G. H. Corrosion inhibition performance and computational studies of pyridine and pyran derivatives for API X-65 steel in 6 M H₂SO₄. *J. Ind. Eng. Chem.* **97**, 523–538 (2021).
- Henry, G. D. D. Novo synthesis of substituted pyridines. *Tetrahedron* **60**, 6043–6061 (2004).
- Jones, G. Comprehensive heterocyclic chemistry II. Pyridines and their benzo derivatives synthesis. *Elsevier* **5**(05), 167–243 (1996).
- Joseph, P. M. Quinoline, quinazoline and acridone alkaloids. *Nat. Prod. Rep.* **22**, 627–646 (2005).
- Movassaghi, M., Hill, M. D. & Ahmad, O. K. Direct synthesis of pyridine derivatives. *J. Am. Chem. Soc.* **129**, 10096–10097 (2007).
- Allaka, T. R. & Katari, N. K. Chapter 17-Synthesis of pyridine derivatives for diverse biological activity profiles: A review. *Recent Dev. Synthesis Appl. Pyridines*, 605–625 (2023).
- Mohamed, E. A., Ismail, N. S. M., Hagrass, M. & Refaat, H. Medicinal attributes of pyridine scaffold as anticancer targeting agents. *Futur. J. Pharm. Sci.* **7**, 1–17 (2021).
- Aliabadi, A., Motieyan, E., Hosseinabadi, F., Ghadermazi, M. & Abdolmaleki, S. One-pot synthesis, crystallographic characterization, evaluation as in vitro antibacterial and cytotoxic agents of two mercury (II) complexes containing pyridine dicarboxylic acid derivatives. *J. Mol. Struct.* **1226**, 129405 (2021).
- Chen, Y.-J. *et al.* The anti-fibrotic and anti-inflammatory effects of 2, 4-diamino-5-(1-hydroxynaphthalen-2-yl)-5H-chromeno [2,3-b] pyriine-3-carbonitrile in corneal fibroblasts. *Pharmacol. Rep.* **72**, 115–125 (2020).
- Ali, E. M. H. *et al.* Design, synthesis and anti-inflammatory activity of imidazol-5-yl pyridine derivatives as p38 α /MAPK14 inhibitor. *Bioorg. Med. Chem.* **31**, 115969 (2021).
- Bass, A. K. *et al.* 3-Cyano-2-oxa-pyridines: A promising template for diverse pharmacological activities. *J. Adv. Biomed. Pharm. Sci.* **4**, 81–86 (2021).
- Hammoudi, N. *et al.* In silico drug discovery of IKK- β inhibitors from 2-amino-3-cyano-4-alkyl-6-(2-hydroxyphenyl) pyridine derivatives based on QSAR, docking, molecular dynamics and drug-likeness evaluation studies. *J. Biomol. Struct. Dyn.* **40**, 1–17 (2022).
- Sugiyama, S. *et al.* Discovery of novel HIV-1 integrase-LEDGF/p75 allosteric inhibitors based on a pyridine scaffold forming an intramolecular hydrogen bond. *Bioorg. Med. Chem. Lett.* **33**, 127742 (2021).
- Gouda, M. A., Berghot, M. A., Abd El Ghani, G. E. & Khalil, A. M. Chemistry of 2-amino-3-cyanopyridines. *Synth. Commun.* **44**, 297–330 (2014).
- Manna, K., Ghosh, P. S., Das, M., Banik, U. & Das, A. 2-amino-3-cyanopyridine: A bioactive scaffold. *IJPSR* **5**, 2158–2163 (2014).
- Zhang, F. *et al.* Synthesis and anti-tumor activity of 2-amino-3-cyano-6-(1H-indol-3-yl)-4-phenylpyridine derivatives in vitro. *Eur. J. Med. Chem.* **46**, 3149–3157 (2011).
- Hosseinzadeh, Z., Razzaghi-Asl, N., Ramazani, A., Aghahosseini, H. & Ramazani, A. Synthesis, cytotoxic assessment, and molecular docking studies of 2,6-diaryl-substituted pyridine and 3,4-dihydropyrimidine-2(1H)-one scaffolds. *Turk J. Chem.* **44**, 194–213 (2020).
- Karczl, D. *et al.* Structural features of 1,3,4-thiadiazole-derived ligands and their Zn(II) and Cu(II) complexes which demonstrate synergistic antibacterial effects with kanamycin. *Int. J. Mol. Sci.* **21**, 5735 (2020).
- Matwijczuk, A., Kluczyk, D., Górecki, A., Niewiadomy, A. & Gagoś, M. Spectroscopic studies of fluorescence effects in bioactive 4-(5-heptyl-1,3,4-thiadiazol-2-yl)benzene-1,3-diol and 4-(5-methyl-1,3,4-thiadiazol-2-yl)benzene-1,3-diol molecules induced by pH changes in aqueous solutions. *J. Fluoresc.* **27**, 1201–1212 (2017).
- Anwer, K. E. & Sayed, G. H. Conventional and microwave reactions of 1, 3-diaryl-5, 4-enaminonitrile-pyrazole derivative with expected antimicrobial and anticancer activities. *J. Heterocycl. Chem.* **57**, 2339–2353 (2020).
- Zuliani, A. *et al.* Improving the electrocatalytic performance of sustainable Co/carbon materials for the oxygen evolution reaction by ultrasound and microwave assisted synthesis. *Sustain. Energy Fuels* **5**, 720–731 (2021).
- Anwer, K. E., Sayed, G. H., Kozakiewicz-Piekarz, A. & Ramadan, R. M. Novel annulated thiophene derivatives: Synthesis, spectroscopic, X-ray, Hirshfeld surface analysis, DFT, biological, cytotoxic and molecular docking studies. *J. Mol. Struct.* **1276**, 134798 (2023).
- Anwer, K. E., Sayed, G. H. & Ramadan, R. M. Synthesis, spectroscopic, DFT calculations, biological activities and molecular docking studies of new isoxazolone, pyrazolone, triazine, triazole and amide derivatives. *J. Mol. Struct.* **1256**, 132513 (2022).
- Sayed, G. H., Azab, M. E. & Anwer, K. E. Conventional and microwave-assisted synthesis and biological activity study of novel heterocycles containing pyran moiety. *J. Heterocycl. Chem.* **56**, 2121–2133 (2019).
- Frisch, M. J., Schlegel, H. B., Scuseria, G. E., Robb, M. A., Cheeseman, J. R., Scalmani, G., Barone, V., Mennucci, B., Petersson, G. A. *et al.* Gaussian Inc., Wallingford, CT (2009).
- Mohamed, R. G. *et al.* Spectroscopic, DFT, biological, DNA binding and antioxidant studies of some metal chelates with a novel thiazole derived Schiff base. *J. Coord. Chem.* **71**, 3665–3688 (2018).
- Silverstein, R. M., Webster, F. X., Kiemle, D. J. & Bryce, D.L. in *Spectrometric Identification of Organic Compounds*, 8th Ed., (Wiley, 2014).
- Gan, B. K. *et al.* Targeted delivery of 5-fluorouracil-1-acetic acid (5-FA) to cancer cells overexpressing epithelial growth factor receptor (EGFR) using virus-like nanoparticles. *Sci. Rep.* **10**, 1–15 (2020).
- Qiao, L. L., Yao, W. J., Zhang, Z. Q., Yang, X. & Zhao, M. X. The biological activity research of the nano-drugs based on 5-fluorouracil-modified quantum dots. *Int. J. Nanomedicine* **15**, 2765 (2020).
- Sayed, G. H., Azab, M. E., Negm, N. A. & Anwer, K. E. Antimicrobial and cytotoxic activities of some novel heterocycles bearing pyrazole moiety. *J. Heterocycl. Chem.* **55**, 1615–1625 (2018).
- Gupta, R., Sheikh, H. N., Kalsotra, B. L. & Singh, V. Synthesis and characterization of isothiocyanato complexes of dioxotungsten(VI) with mannich base ligands: Precursors for the preparation of pure phase nanosized tungsten(VI) trioxide Dioxotungsten(VI) isothiocyanato complexes with mannich bases: Precursors for WO₃. *J. Saudi Chem. Soc.* **20**, 291–302 (2016).
- Ojha, M., Yadav, D., Kumar, A., Dasgupta, S. & Yadav, R. 1,8-Naphthyridine derivatives: A privileged scaffold for versatile biological activities. *Mini Rev. Med. Chem.* **21**, 586–601 (2021).
- Nguyen, P. L., Bui, B. P., Lee, H. & Cho, J. A novel 1,8-naphthyridine-2-carboxamide derivative attenuates inflammatory responses and cell migration in LPS-treated BV2 cells via the suppression of ROS generation and TLR4/Myd88/NF- κ B signaling pathway. *Int. J. Mol. Sci.* **22**, 2527 (2021).
- Ašanin, D. P. *et al.* Structural characterization, antimicrobial activity and BSA/DNA binding affinity of new silver (I) complexes with thianthrene and 1, 8-naphthyridine. *Molecules* **26**, 2021 (2021).
- Jyothi, K. L. *et al.* Structural elucidation, theoretical insights and thermal properties of three novel multicomponent molecular forms of gallic acid with hydroxypyridines. *J. Mol. Struct.* **1207**, 127828 (2020).
- Ramadan, R. M., El-Medani, S. M., Makhlof, A. A., Moustafa, H., Afifi, M. A., Haukka, M. & Abdel Aziz, A. A. Spectroscopic, DFT, non-linear optical properties and in vitro biological studies of Co(II), Ni(II) and Cu(II) complexes of hydrazide Schiff base derivatives. *Appl. Organometal. Chem.* e6246 (2021).
- Shruthi, C. *et al.* Molecular structure, Hirshfeld surface and density functional theoretical analysis of a NLO active chalcone derivative single crystal-A quantum chemical approach. *J. Mol. Struct.* **1228**, 129739 (2021).
- El-Medani, S. M. *et al.* Spectroscopic, crystal structural, theoretical and biological studies of phenylacetohydrazide Schiff base derivatives and their copper complexes. *J. Mol. Struct.* **1208**, 127860 (2020).

39. Hassen, S., Chebbi, H., Zid, M. F. & Arfaoui, Y. Assembly and weak interactions in the crystal structure of 2-amino-4-(3-bromophenyl)-1,3,5-triazinobenzimidazolium chloride studied by X-ray diffraction, vibrational spectroscopy, Hirshfeld surface analysis and DFT calculations. *J. Mol. Struct.* **1179**, 678–684 (2019).
40. Yildiz, M. *et al.* Synthesis, biological activity, DNA binding and anion sensors, molecular structure and quantum chemical studies of a novel bidentate Schiff base derived from 3,5-bis(trifluoromethyl)aniline and salicylaldehyde. *J. Mol. Struct.* **1094**, 148–160 (2015).
41. Geesi, M. H. *et al.* Synthesis, antibacterial evaluation, Raman, crystal structure and hirshfeld surface analysis of a new 3-(4-fluorophenyl)-6-methyl-2-(propylthio) quinazolin-4 (3H)-one. *J. Mol. Struct.* **1215**, 128265 (2020).
42. Raja, N., Ramesh, R. & Liu, Y. Paramagnetic ruthenium(III) complexes bearing O, O chelating ligands: Synthesis, spectra, molecular structure and electron transfer properties. *Polyhedron* **31**, 196–201 (2012).
43. Ramadan, R. M., Noureldeen, A. F. H., Abo-Aly, M. M. & El-Medani, S. M. Spectroscopic, DFT analysis, antimicrobial and cytotoxicity studies of three gold(III) complexes. *Inorg. Nano-Metal Chem.* **52**, 213–225 (2022).
44. Harrold, M. W. & Zavod, R. M. in *Basic Concepts in Medicinal Chemistry*. (American Society for Health-System Pharmacists, 2013).
45. Abdel Ghani, N. T. & Mansour, A. M. Structural and in vitro cytotoxicity studies on 1H-benzimidazol-2-ylmethyl-N-phenyl amine and its Pd(II) and Pt(II) complexes. *Spectrochim. Acta Part A* **81**, 529–543 (2011).
46. Yamaguchi, T., Takamura, H., Matoba, T. & Terao, J. HPLC method for evaluation of the free radical-scavenging activity of foods by using 1,1-diphenyl-2-picrylhydrazyl. *Biosci. Biotechnol. Biochem.* **62**, 1201–1204 (1988).
47. Tiwari, O. P. & Tripathi, Y. B. Antioxidant properties of different fractions of *Vitex negundo* Linn. *Food Chem.* **100**, 1170–1176 (2007).
48. Nicolaidis, D. N., Gautam, D. R., Litinas, K. E., Hadjipavlou-Litina, D. J. & Fylaktakidou, K. C. Synthesis and evaluation of the antioxidant and antiinflammatory activities of some benzo[*l*]khellactone derivatives and analogues. *Eur. J. Med. Chem.* **39**, 323–332 (2004).
49. Kim, J.-S. Radical scavenging capacity and antioxidant activity of the E Vitamer fraction in rice bran. *J. Food Sci.* **70**, C208–C213 (2005).
50. Madigan, M. T., Martinko, J. M., Bender, K. S., Buckley, D. H., Stahl, D. A. & Brock, T. in *Brock Biology of Microorganisms*, 14th Ed., (Pearson, 2014).
51. Ramadan, R. M. & Noureldeen, A. F. H. Molecular docking and drug design of schiff base metal complexes. In *Structural and Biological Applications of Schiff Base Metal Complexes*, (eds Jain, P. & Singh, P.) (CRC Press, Taylor & Francis Group, London, 2023).

Author contributions

K.E.A and Z.K.H. did the experimental work, analysis of the compounds, prepared figures and wrote the first draft. R.M.R. did the theoretical calculations, wrote and revised the final main manuscript text. All authors reviewed the final manuscript.

Funding

Open access funding provided by The Science, Technology & Innovation Funding Authority (STDF) in cooperation with The Egyptian Knowledge Bank (EKB). Authors have received no funds for this research.

Competing interests

The authors declare no competing interests.

Additional information

Supplementary Information The online version contains supplementary material available at <https://doi.org/10.1038/s41598-023-42714-w>.

Correspondence and requests for materials should be addressed to R.M.R.

Reprints and permissions information is available at www.nature.com/reprints.

Publisher's note Springer Nature remains neutral with regard to jurisdictional claims in published maps and institutional affiliations.



Open Access This article is licensed under a Creative Commons Attribution 4.0 International License, which permits use, sharing, adaptation, distribution and reproduction in any medium or format, as long as you give appropriate credit to the original author(s) and the source, provide a link to the Creative Commons licence, and indicate if changes were made. The images or other third party material in this article are included in the article's Creative Commons licence, unless indicated otherwise in a credit line to the material. If material is not included in the article's Creative Commons licence and your intended use is not permitted by statutory regulation or exceeds the permitted use, you will need to obtain permission directly from the copyright holder. To view a copy of this licence, visit <http://creativecommons.org/licenses/by/4.0/>.

© The Author(s) 2023